PERGAMON

Journal of Structural Geology 24 (2002) 1541–1567

JOURNAL OF STRUCTURAL GEOLOGY

www.elsevier.com/locate/jstrugeo

Studies of strain and rheology of conglomerates

Susan H. Treagus*, Jack E. Treagus

Department of Earth Sciences, University of Manchester, Manchester M13 9PL, UK

Received 7 July 2001; accepted 15 November 2001

Abstract

Conglomerates can show significant strain variations among their component rock types. Previous studies have exploited this feature as a method of quantifying the effective viscosity ratios among different rock types, using inclusion–matrix models that we review here. We further investigate the rheology of conglomerates via models of multiphase mixtures of spherical clasts with varying phase fractions. Using idealised models with two to four phases, we can quantify the influence of phase viscosities and volume fractions on the bulk viscosity, and reveal how this controls the strain partitioning among the different phases.

We consider practical methods of analysing conglomerates, and choose R_f-ϕ analysis for measuring clast strain, and Fry analysis for whole-rock strain. The methods are illustrated through case studies of two very different conglomerates, the Port Askaig Tillite, Scotland, and Cesson Conglomerate, Brittany. We define the important rock phases in each, and assess their strain variations. Although providing strain measurements of regional interest, our main purpose is to quantify the viscosity ratios among the component rocks. We find that among the most common rock types (semipelite, quartzite, psammite, volcanics, granite), the viscosity ratios span about one order of magnitude, agreeing with previous studies. These small numerical values for viscosity ratios among many rock types, in many conglomerates, lead us to conclude that these rocks each deformed at approximately constant viscosity: i.e. as linearly viscous, rather than according to a power law.

Keywords: Conglomerate; Strain; Rheology; Rock viscosity ratios

1. Introduction: conglomerates and strain analysis

Conglomerates are commonly used for geological strain analysis, and their regular occurrence in the geological succession makes them promising strain marker horizons. Many of the current techniques for geological strain analysis have developed from early studies of deformed conglomerates. For example, the first quantitative three-dimensional study of a deformed conglomerate was Flinn's analysis of the Funzie conglomerate of Shetland (Flinn, 1956). In early studies by Hossack (1968), Burns and Spry (1969) and Gay (1969), it was largely assumed that the ellipsoidal shapes of the conglomerate clasts reflected the strain, as if the clasts were initially spherical. However, it was understood that this strain did not necessarily reflect the whole-rock strain, and it was this difference that prompted Gay's analysis of conglomerates in terms of viscosity contrasts and modelling (Gay, 1968a,b, 1969), discussed in Section 2.

Ramsay (1967) and Ramsay and Huber (1983) each provide comprehensive reviews of methods in the analysis of strain in conglomerates. Probably the most widely used method is R_f-ϕ analysis (Ramsay, 1967; Dunnet, 1969; Lisle, 1985), making use of aspect ratios and orientations of the pebbles in several planar sections of a conglomerate outcrop, either from measurements in the field or from photographs. R_f-ϕ analysis has its basis in the concept of passive deformation of initially elliptical objects, and so this method does not require the assumptions that the pebbles were initially spherical, and thus circular in section. Instead, the R_f-ϕ data are assumed to represent a statistical sample of initially randomly oriented elliptical objects of different aspect ratio (R_i). There are various ways to determine a statistical strain ratio (R_S) from an R_f-ϕ plot (Ramsay, 1967; Ramsay and Huber, 1983; Lisle, 1985), including taking the geometric mean of the minimum and maximum R_f points on an ordinate line of symmetry. On the basis of artificial simulations of deformed elliptical markers, Lisle (1979) concluded that the *harmonic mean* of all the R_f values gave the closest result to the real applied strain, better than either the arithmetic or geometric means (although none were good estimates where the initial shape factor was large and applied strain relatively small).

For conglomerates that are almost entirely made up of clasts which can be measured, the strain determined from

* Corresponding author. Tel.: +44-(0)161-275-3804; fax: +44-(0)161-275-3947.

E-mail address: s.treagus@man.ac.uk (S.H. Treagus).

0191-8141/02/$ - see front matter
PII: S0191-8141(01)00162-6

their R_f-ϕ analysis might be thought to yield a good approximation to the bulk whole-rock strain. However, even a well-packed clast-supported conglomerate is likely to have a significant volume that is matrix, varying according to the regularity and degree of clast packing. If the clasts are uniform-sized spheres, the maximum possible clast fraction is 52% for perfect cubic packing, and 74% for hexagonal packing (Leeder, 1982, p. 42). Rocks containing clasts with irregular shapes, and/or a significant variation in clast size, have theoretically higher maximum packing values. However, our measurements of natural conglomerates made in connection with this paper suggest that the pebble fraction rarely exceeds 50% of the rock volume, and is usually considerably less, which means that >50% of the conglomerate comprises the rock matrix. This matrix might be a finer-grained fragmental rock, with similar rock types to those in the pebble clast fraction, or have a different lithology.

It follows that the strain determined by R_f-ϕ analysis of pebbles in conglomerates will generally be only a partial measure of the whole-rock strain. In most cases, it will be an underestimate, because pebbles in conglomerates are more usually 'competent' rock types such as quartzites, chert, volcanics, or granites, deformed to a lesser degree than the matrix rock. The differences in strain recorded among clasts of different rock types have been described and quantified in a number of studies of deformed conglomerates (Gay, 1968a,b, 1969; Huber-Aleffi, 1982; Lisle et al. 1983; Freeman and Lisle, 1987), and provide important evidence of viscosity ratios among different rock types, as reviewed in Section 2, and pursued further in this paper.

If the strain determined for a particular population of clasts in a conglomerate is not the whole-rock strain, how might the bulk strain in these kinds of rocks be determined? The most promising methods would appear to be those that use spatial information, such as various 'centre-to-centre' analyses (Ramsay and Huber, 1983, pp. 110–112). Of these, Fry analysis is the best known (Fry, 1979): but although the Fry method and its modifications have been well discussed in theory (Fry, 1979; Erslev, 1988; Erslev and Ge, 1990; McNaught, 1994), we are unaware of any published applications of the techniques to the analysis of whole-rock strain in conglomerates. It is arguable whether a simple manual Fry analysis is strictly valid for these kinds of rocks, especially where there is a wide range of clast sizes and rock types, but it may nevertheless provide the best first-order method.

R_f-ϕ and Fry analyses are considerably simplified by using personal computers and modern interactive computer software. For R_f-ϕ analysis of conglomerates, traces of clast outlines can be scanned and input into *NIH Image*(the US National Institute of Health Mac-based image analysis software: http://rsb.info.nih.gov/nih-image/), which then automatically finds best-fit ellipses and produces axial measurements and orientations (see Bjornerud and Boyer, 1996; Bons and Jessell, 1996; De Paor, 1996). For Fry analysis, the *Fry 5.9.3* software developed by De Paor and Simpson (information: http://www.scienceprof.com) enables the user to create digital Fry plots interactively from scanned photographic images of rock outcrops or thin sections. These methods are followed in the conglomerate case studies in this paper.

Another method of determining a whole-rock conglomerate strain, by 'summing' the strains of the component parts, will be discussed later in this paper. We should, however, note an interesting method used by Huber-Aleffi (1982) to calculate bulk (whole rock) strain at different localitities in the Alpine Lebendun conglomerate. She subdivided this rock into four distinct rock-type phases: aplite, granite-gneiss, augen gneiss and mica-schist. The strain ratio was determined for each rock type (at each locality), and then plotted against the 'rest of rock' strain ratio (taken as the geometric mean of the other three phases). A curve was drawn through the three points, and the point where it crossed the graph diagonal located the R value of the 'whole rock strain'. The method would appear to give the same result as taking the geometric mean of the strains for the four rock types at each locality. However, either method is probably only valid for determining the bulk strain if the four rock groups occupy equal fractions of the whole rock. We are not aware of any published studies that make specific use of area or volume fractions of component rock types, to calculate a 'weighted' whole rock strain, in the manner that will be discussed later in this paper.

2. Rheology of conglomerates: viscosity contrasts

2.1. Inclusion–matrix theory

Gay (1968a,b, 1969) was the first to investigate ways to quantify the differences between clast strain and whole-rock (bulk) strain in conglomerates, in terms of viscosity ratios. He developed a theory for the two-dimensional deformation of ellipsoidal objects in a contrasting viscous matrix, and applied this to published strain data for deformed conglomerates, and to his own field data, to determine viscosity ratios for various rock types (Table 1a). In reviews elsewhere (Treagus and Lan, 2000; Treagus and Treagus, 2001; Treagus, 2002), we have discussed the differences between Gay's (1968a) formula and the theoretical analyses of Eshelby (1957) and Bilby et al. (1975), and also differences between two-dimensional analyses of circular/elliptical inclusions modelled as cross-sections of cylinders, and three-dimensional analyses of spherical/ellipsoidal inclusions in a matrix (Freeman, 1987; Freeman and Lisle, 1987). In Appendix A, we summarise the main points that are relevant to studies of conglomerates, and develop reasoning for using Gay's (1968a) equation (Eqs. (1) and (A1)) as the most suitable for application to conglomerates.

This states that for an initially circular inclusion in a

Table 1
Viscosity ratios among conglomerate rock types.

(a) After Gay (1968b)

Rock type	Viscosity ratio relative to shale
Shale	1.0
Greywacke	1.2–1.5
Fine quartzite	1.4–2.0
Coarse quartzite	1.8–3.5
Volcanic quartz	4.2–12.0
Schist	1.0
Gneiss	1.3–1.7
Quartz	1.7–2.6

(b) After Lisle et al. (1983)

Rock type	Viscosity ratio relative to whole rock
Quartz	9
Hard leptite	2
Soft leptite	1.4
Halleflinta	1.3
Light shale	0.9
Dark shale	0.85
	Viscosity ratio relative to dark shale
Whole rock	1.2
Quartz	10.6
Hard leptite	2.35
Soft leptite	1.65
Halleflinta	1.53
Light shale	1.06

matrix of contrasting viscosity, in bulk pure shear:

$$\ln R_O = \ln R_S\{5/(3 + 2r)\}, \quad (1)$$

where R_O is the inclusion or object strain ratio (the X/Z stretch ratio), R_S is the bulk X/Z strain ratio (equivalent, here, to the average matrix strain), and r is the viscosity ratio between the inclusion and matrix. This linear $\ln R$ expression is illustrated graphically in Fig. A1. Alternatively, we can write Eq. (1) in terms of the viscosity ratio, r:

$$r = \frac{1}{2}\left(\frac{5\ln R_S}{\ln R_O} - 3\right). \quad (2)$$

2.2. Determinations of viscosity ratios

Use of Eq. (2) to determine viscosity ratios depends on having reliable methods for determining the inclusion strain and bulk strain values to yield their ratio ($\ln R_O/\ln R_S$). Applied to conglomerates, this raises a number of practical problems. In the approaches of Gay (1968a,b) and Lisle et al. (1983), the 'inclusion strain' is not being measured for *one* single isolated (spherical) inclusion in a matrix, in accordance with the inclusion–matrix modelling and mathematics outlined in Appendix A. Instead, the 'inclusion strain' is determined as an average strain for a *population of clasts* of a particular rock-type. Individually and collectively, these are considered to have deformed in a 'matrix' that has a different viscosity, where the 'matrix' here has the properties of the 'whole rock' (rather than the true rock matrix of the conglomerate). Thus the viscosity ratios that are determined in studies of conglomerates by Gay (1968b) and Lisle et al. (1983) (Table 1), apply to clasts of a particular rock-type relative to the bulk whole-rock viscosity. In Section 3, next, we investigate methods of quantifying the bulk viscosity of conglomerates and multiphase mixtures.

Table 1 provides a summary of the viscosity ratios among different clast rock-types in conglomerates, determined by Gay (1968a,b) and by Lisle et al. (1983) from inclusion–matrix modelling. Although their theories and methods of calculation differ, the numerical results are not significantly different. Both approaches depend on the ability to measure the strain in populations of clasts of particular types, to arrive at R_O values for a number of specific rock-types (for use in Eq. (1) or (2)). However, the problem found in both these studies was in having no straightforward way to measure the bulk whole rock strain (R_S), and this they tackled in different ways. Gay's (1968b) method was based on finding value ranges for viscosity ratios, by adopting limiting values of 1 and 100 for one clast type relative to whole rock. Lisle et al. (1983) employed a computer program for integrating the equation given by Bilby and Kolbuszewski (1977), to unstrain the R_f-ϕ data points numerically for groups of clasts by rock-type, trying different values of bulk strain (R_S) and of clast/rock viscosity ratio (r). Lisle et al. (1983, fig. 5) sought the best numerical solutions for which the unstrained R_f-ϕ distribution for each population becomes closest to random (the assumed initial state), revealing value ranges for R_S and r for five different clast rock types (Table 1b). Their calculated R_S in two principal sections is the numerical value that gives the best result to satisfy all five rock types to give consistent r values. The r values can then be written as mutual viscosity ratios for pairs of specific rock types, as reproduced in Table 1b 'relative to shale'. We will present a simpler method later in this paper, and will then compare our results with those summarised in Table 1.

2.3. Rock viscosity and Newtonian modelling

The viscosity ratios derived by the foregoing analyses were based on the assumption that the clasts and their 'matrix' behaved as Newtonian fluids, with constant viscosity over the finite deformation. In strict terms, *viscosity* can only ever refer to instantaneous flow properties, and thus only relates to infinitesimal deformation. Only if the rocks have constant viscosities over the duration of the geological strain, as is the case for Newtonian fluids, are viscosity ratios strictly calculable from the *finite* strain relationships given above.

A considerable quantity of information on deformation of rocks and minerals in the laboratory (see reviews: Carter and Tsenn, 1987; Kirkby and Kronenberg, 1987; Rutter,

1993; Kohlstedt et al., 1995) would seem to support the conclusion that rocks do not generally flow as Newtonian fluids at laboratory strain-rates, and can exhibit a wide range of creep behaviour associated with different types of deformation mechanism. Whether this variation in behaviour is truly the case for many crustal rocks, at the rates, scales and conditions of geological deformation, is best answered by analysis of natural geological structures that yield information on the rheology of rocks, such as studies of conglomerates. It might seem improbable that all the component rocks in conglomerates have behaved as approximately linearly viscous, as required by the preceding theoretical modelling. However, if most rocks were non-Newtonian, we should expect a wide variation of effective viscosity ratios among different rocks, under different conditions. This is not apparent from studies of conglomerates (Table 1), or from folded layers (Shimamoto and Hara, 1976), or values estimated from cleavage refraction (Treagus, 1999). For this reason, we justify modelling all the rock phases in conglomerates as approximately Newtonian, with a characteristic viscosity. Even with this assumption, and with the simplification that conglomerates are uniform mixtures of spherical clasts, it is not a trivial matter to define the bulk viscosity, as discussed next.

3. Rheology of conglomerates: bulk properties

3.1. Modelling mixtures

The methods described in the preceding section for determining viscosity ratios of specific clast rock types, relative to the bulk rock viscosity, raise broader questions about the bulk rheology of conglomerates; and of mixtures of several phases in general. In a companion study, Treagus (2002) reviews current methods of quantifying the bulk properties of two-phase aggregates or mixtures. This subject embraces approaches in the materials sciences and geological sciences, and is based on the principles of statistical behaviour of two-phase elastic composites and their 'self consistent mechanics' (Hill, 1965; Hashin, 1983 and references therein), but applied to viscous mixtures. Treagus (2002) considers regular-patterned two-phase mixtures with various clast shapes (circles, ellipses, squares, rhombs), in two dimensions, and develops algebra for describing the bulk viscosity in terms of the viscosities of the two phases, their area fractions, and a 'clast shape factor'. In this approach, each clast is effectively modelled as if it were an 'isolated inclusion' with contrasting properties to the 'matrix', whose rheology is that of the mixture. In this paper on conglomerates, we are interested in three-dimensional multiphase mixtures of clasts that were initially originally spherical or ellipsoidal. (A population of initially randomly oriented ellipsoids, as assumed in R_f-ϕ analysis discussed earlier, can be considered as statistically spherical.) In Appendix B, we develop theoretical modelling for mixtures of this kind, beginning with two-phase systems (after Treagus, 2002), and then considering a number of types of multiphase mixtures. We consider their relevance to conglomerates, below.

3.2. Applications of multiphase models to conglomerates

Applying any of the models in Appendix B to real conglomerates, or other types of rocks, involves first assuming (1) pure shear, (2) plane strain, (3) Newtonian viscous phases, (4) statistically uniform mixtures, and (5) statistically spherical clast or grain shapes. We then need to consider the make-up of various conglomerates in terms of the numbers of phases, their fractions, and their mutual viscosity contrasts. No account is taken in the preceding modelling for variations of clast size; however, for conglomerates, it is not unreasonable to assume that there are one or more definable fractions of similar-sized clasts in a matrix phase that can be considered a different material. In practice, this matrix may itself comprise a number of different rock or mineral phases, on a particular scale; but relative to pebble-sized clasts, it may be justified to model this as a uniform phase with a definable viscosity.

Some kinds of conglomerates might be considered to approximate a *two-phase mixture*, with a statistically spherical clast phase of a certain fraction, in a matrix phase with different material properties, where both phases are Newtonian viscous. Straightforward algebraic relationships outlined in Appendix B.1 then allow the bulk viscosity for these mixtures to be calculated, in terms of the two-phase viscosity contrast (m) and each volume fraction (α_1, α_2). As expected, the bulk viscosity progressively increases, with increasing fraction of the stiffer phase. For example, a two-phase conglomerate-like mixture, with a competent/incompetent viscosity ratio of $m = 10$ (Fig. B1), with a competent clast fraction of $\alpha_2 = 0.3$, and an incompetent matrix fraction of $\alpha_1 = 0.7$, would have a bulk viscosity of about twice that of the matrix viscosity: i.e. a β value of 2 from Eq. (B5). Writing each phase viscosity ratio relative to the whole mixture (i.e. as an r value), the clast fraction has $r = 5$, and the matrix has $r = 0.5$. A similar rock with equal clast and matrix fractions ($\alpha_1 = \alpha_2 = 0.5$) would be a stiffer mixture, with $\beta = 3.7$, and a clast/rock viscosity ratio of $r = 2.7$ (and for matrix, $r = 0.27$) (Fig. B1).

These two numerical examples illustrate the importance of the volume fractions of the two phases on the mixture properties, and thus on the effective viscosity contrasts of a clast fraction to the whole rock (r). The value of r controls the strain differences and partitioning of strain in the system, as given in Eq. (1) (see Appendix A). Taking a bulk strain of $R_S = 4$, we find that for the first example (0.3 competent fraction; clast/matrix viscosity contrast of $m = 10$), the clast strain (ratio) is $R = 1.7$, and the matrix strain is $R = 5.7$. In the 0.5 fraction mixture, the clast strain is $R = 2.3$, and the matrix strain ratio is $R = 7.1$. For both examples, therefore, the strain determined

for the competent clast fraction, such as by R_f-ϕ analysis, would *underestimate* the whole-rock strain significantly. If the strain could be determined for the incompetent matrix fraction (e.g. by Fry analysis), this would overestimate the whole-rock strain.

The types of multiphase mixtures considered in Appendix B.3 and Fig. B2, with equal fractions of *three or four phases* in equal factors of increasing viscosity, might not appear to be particularly well-suited for modelling natural conglomerates. However, they provide useful indicators of which phases and variables might have important controls on the bulk rheology, and may provide approximations that could be useful for multiphase mixture in general. Fig. B2b compares the normalised bulk viscosity (β) with the *maximum* phase viscosity ratio, M, and the similarity of curves for the three- and four-phase mixtures suggests that the *number* of intermediate phases in a multiphase mixture is less important than the maximum viscosity contrast, M. We derived the approximation of $\beta \cong M^{0.55}$ (Appendix B.3) for N-phase mixtures with equal phase fractions ($\alpha_n = 1/N$) of this type. This suggests that the number of phases intermediate between the weakest and stiffest is relatively unimportant, so long as the 'fragmentation' of the mixture is by equal fractions and equal factors of viscosity change. We find that $\beta \cong 3.5$, for a mixture with $M = 10$, and so the most competent fraction would have a viscosity contrast to the bulk viscosity of $r \equiv M/\beta \cong 2.9$. For $M = 100$, we determine $\beta \cong 13.2$, and thus a viscosity contrast of the most competent phase (to the bulk) of $r \cong 7.6$. For both examples, we therefore find $r < 10$, which supports the values of viscosity contrasts (relative to the whole rock) within one order of magnitude, as were shown in Table 1 earlier for clasts in conglomerates.

Matrix-supported conglomerates, especially those such as tillites that have a large volumetric fraction of matrix, and widely separated pebbles and boulders, might reasonably be modelled as weak suspensions of clasts in a matrix. For this kind of rock, the three-phase model we considered in Appendix B.4 could be useful: a mixture with a varying matrix phase fraction (phase 1; the least viscous, or incompetent), and two different competent clast phases (phases 2 and 3). For example, for a mixture with triple viscosity ratio of 1:10:100 (Fig. B3), with a total clast fraction of 0.3 ($\alpha_1 = 0.7$; $\alpha_2 = \alpha_3 = 0.15$), we find the bulk viscosity of the mixture is $\beta \cong 2.5$, and the viscosity ratios relative to the bulk viscosity would be $r \cong 0.4$ for phase 1, ~4 for phase 2, and ~40 for phase 3. According to Eq. (1), phase 3 would be virtually undeformed, thus appearing rigid. For the example of $R_S = 4$, we calculate phase strains of $R = 6$ for phase 1 (matrix), $R = 2$ for clast phase 2, and $R = 1.1$ for clast phase 3.

Now consider a similar idealised three-phase conglomerate, but not such a weak suspension: one with equal matrix and clast fractions ($\alpha_1 = 0.5$; $\alpha_2 = \alpha_3 = 0.25$). This might simulate a reasonable limit for a well-packed pebble fraction in a clast-supported conglomerate, as discussed earlier. It makes a stiffer mixture, and the numerical values now work out quite differently from the preceding example, using the same triple viscosity ratio of 1:10:100 (see Fig. B3). The bulk viscosity is given by $\beta \cong 6.5$, and the effective viscosity ratios are $r \cong 0.15$ for phase 1, $r \cong 1.5$ for phase 2, and $r \cong 15.4$ for phase 3. Considering again a bulk strain ratio of $R_S = 4$, we now find phase strains of $R = 8.2$ in the matrix (phase 1), which is a considerable intensification of the strain, $R = 3.2$ in phase 2 (now closer to the bulk strain), and $R = 1.2$ in phase 3 (negligible strain).

The numerical values for these two three-phase 'rocks' illustrate the interrelationship of the effective viscosity contrasts, the 'strain partitioning' among the phases, and the fractions of each phase. For a decreasing fraction of the incompetent matrix, there is an increased concentration of strain in this component, a progressively higher strain than the bulk strain. From the appearance of such a 'rock', it would not necessarily be obvious which of the three phases (if any) best approximates the whole-rock strain.

4. Conglomerate case studies: analytical methods

4.1. General procedures

Through analyses of deformed conglomerates that follow in Sections 5 and 6, using the modelling in Sections 2 and 3 (plus Appendices A and B), we will attempt to draw some conclusions about the rheology of real conglomerates of different types. We seek to use the specific variation of strain among different clast rock types, or between the matrix and clast population, or in a clast fraction relative to the whole rock, to put numerical values to the viscosity contrasts among the rock components. This may provide information on the bulk rheology of a conglomerate in terms to its component parts, revealing whether the whole-rock properties of a particular conglomerate are dominated by a particular clast fraction; or by the matrix; or neither.

A standard procedure was followed in all our field studies. We sought clean planar exposures, preferably close to the principal macroscopic fabric planes in the rock (taking cleavage as the XY plane, and its stretching lineation as X); then made field measurements of clast long/short axes, photographed the rock surfaces for later strain analysis, and obtained samples for sectioning. We tried to analyse strain on different scales, from field, hand specimen and thin section data, and using different procedures, as described in Section 1 and expanded upon next.

4.2. Procedures of rock and strain analysis

We use two procedures of direct strain analysis, as introduced with citations in Section 1: R_f-ϕ analysis of clasts, and Fry analysis of whole rock. Some indirect methods of determining whole rock or bulk strain are then discussed.

R_f-ϕ analysis of clasts uses clast outlines traced from

photographs or hand specimens, analysed using *NIH Image* (see Section 1), which automatically approximates shapes to ellipses. Such analyses produce tabulated measurements of clast long and short axes and long-axis orientation, suitable for importing into a drawing package to produce the required R_f-ϕ graphs (e.g. for comparison with the templates in Lisle, 1985), or for mathematical and statistical calculations such as the determination of arithmetic, geometric and harmonic means for each R_f population. This method of R_f-ϕ analysis was applied to all clasts collectively from a photograph or rock specimen, and also to groups of clasts of similar rock type (aided by later petrographic identification). In some cases, the number of measurements for a particular rock type in the exposure or photograph did not reach the suggested 30 + recommended for strain analysis (see Lisle, 1985, p. 10), in which case the average strains could be rather crude estimates. Nevertheless, we found that the values of the geometric mean, the harmonic mean and the median were generally close. We follow Lisle (1979) in using the harmonic mean of all R_f values as the preferred method of finding the *average strain* (ratio, R) for a particular population: for all clasts, and also for clasts grouped by rock type.

Fry analysis was applied on different scales, from field photographs of conglomerate exposures, to photographs or direct scans of rock slices. In theory, this might allow us to determine the bulk strain (R_S) of a rock or area of exposure; or alternatively, of a particular rock such as the matrix, on the scale of a thin section. We used D.G. De Paor's Earth'nWare automated software *Fry 5.9.3*, as introduced in Section 1, and the method can be applied to any pict or tiff image. The centres of all identifiable clasts or grains over a chosen size range were used, on the assumption (Fry, 1979) that these were initially random, not clustered. *Fry 5.9.3* allows the user to click the centres of clasts or particles, and these points are recorded and used to produce a digital Fry plot. A central ellipse can be drawn in the 'hole' in the centre of the Fry plot, and its size, aspect ratio and orientation changed interactively until it fits the pattern of dots most appropriately. It is left to the user to decide how to fit this 'best ellipse'. For most of our Fry whole-rock analyses, we did not obtain a strong elliptical halo of innermost points of the 'text-book' kind (e.g. Ramsay and Huber, 1983, fig. 7.10): but with sufficient data there was usually a definable vacancy outlined by about a dozen points. We sought the 'best ellipse' to fit the vacancy, by trial and error, that (a) has its long axis subparallel to the macroscopic extension direction or cleavage trace in the image, and (b) fits the maximum number of innermost points in the Fry plot. Despite its imprecision in some cases, we found this method of Fry analysis to be the only practical *direct* method of determining the bulk strain (R_S) for particular images of conglomerates.

An alternative *indirect* approach to determining the bulk strain is to use the fractions of the different rock types and their strains. *Area fractions* are assessed by manual area-counting of field photographs and samples. If the whole rock can be attributed to quantifiable fractions of clast or matrix rock types, a particular conglomerate can then be considered as a multiphase system, as discussed in Section 3. We could in theory then determine $\ln R_S$ as the 'sum of N parts' (cf. Eq. (B8) or (B9)):

$$\ln R_S = \sum_{n=1}^{N} \alpha_n \ln R_n \tag{3}$$

where α_n is the area or volume fraction of each rock phase (summing to one), and R_n is the strain ratio for each phase, such as the harmonic mean values derived from R_f-ϕ analysis described above.

There are a number of difficulties, however, that surround calculations of area fractions of rock types in conglomerates. First is the difficulty of placing accurate figures on the rock proportions, based on sample rock slices or exposure photographs. Manual area counting is tedious, and the results may be too approximate to be useful in calculations. Secondly, in order to equate area with volume fractions in the deformed state, the area counting needs to be performed in the *XZ* principal plane, and to assume either plane strain for all phases, or a three-dimensional strain that has no differential strain in the third dimension. Neither may be strictly true (Freeman, 1987; Freeman and Lisle, 1987), as discussed in Appendix A. The area fractions assessed for *XY* or *YZ* principal planes may give a false impression of the proportions of the different rock types. For example, in the *YZ* plane (whose overall final/initial area is inversely proportional to the bulk X value), rocks that deform by a smaller X than the bulk strain (i.e. competent rock types) could appear to occupy *greater* area fractions of the whole than initially; incompetent rock types conversely would appear to occupy smaller fractions. The opposite is the case on *XY* sections. Thus, in conglomerate case studies where we might choose to use area fractions as an indication of volumetric fractions, and use Eq. (3) as the method of computing the bulk strain, we must take the fractions on *XZ* sections as the most reliable source. Being the most strongly deformed sections, these can prove the most difficult to analyse.

It is worth recalling from Section 1 that the bulk strain, R_S, was considered *unknown* both by Gay (1969) and by Lisle et al. (1983), in their conglomerate studies (see Table 1). Above, we outlined two possible methods for its determination: Fry analyses of the whole rock; or taking the area-weighted mean strain (Eq. (3)). We might also consider a third method, using the harmonic mean of all the R_f clast data: but only if these data are properly representative of *all* the rock components, including the matrix; and if the number of measurements can be assumed representative of their volume fractions.

4.3. Determining viscosity ratios, r

As noted in Section 2, calculation of the viscosity ratio (r)

of a particular rock phase, relative to the bulk whole-rock viscosity, depends on determining values for the strain in the rock phase *and* for the bulk strain (R_S), which may be more difficult to determine. Assuming that we can reliably specify these, we can use Eq. (2). Values of r determined for specified rock types can then be calibrated into viscosity ratios among specific pairs of rock types, such as the values relative to shale or schist given in Table 1. The reciprocals of the r values will provide the numerical values for the bulk rock viscosity, relative to a particular rock phase. Recall that the bulk viscosity normalized to the least viscous phase, which might be the matrix rock, was termed β in Section 6. In two conglomerate case studies, next, we will apply these principles and the strain values determined for different rock components, to estimate the viscosity ratios and bulk rheological properties.

5. Port Askaig Tillite, Scarabus, Islay, Scotland

5.1. Introduction and rock description

This first example is a rather special type of conglomerate, a tillite (Fig. 1), and is particularly suitable for analysis as a clast–matrix system, because it can be modelled as a 'weak suspension'. Our analyses all come from one outcrop of the Port Askaig Tillite Formation on the island of Islay, off the west coast of Scotland (Strathclyde Region). These rocks, at the base of the Argyll Group of the Dalradian Supergroup (late Precambrian to early Cambrian), have been deformed in the Grampian Orogeny (early Ordovician) and affected by lower greenschist facies metamorphism. The Port Askaig Tillite has been described in detail by Spencer (1971, 1981) from the type locality at Port Askaig, on Islay, 10 km NE of our locality. Our exposure is a quarry at NR 351647 by the road to Scarabus Farm (3 km NE of Bridgend), that is particularly suitable for field study, photography and sampling (Fig. 1). (Map and further details are available from the authors.)

The rock corresponds to one of the higher diamictites in the formation, characterised by clasts of grey to pink granite, together with those of creamy, fine-grained, quartzite and grey psammite. The subangular to subrounded clasts are evenly scattered in a siltstone/sandstone matrix. The clasts occupy two distinct size-range fractions, each comprising about 5% by volume of the whole rock. The first set are boulders or cobbles of granite or psammite, from 25 to 35 cm in maximum diameter, which are widely scattered and appear virtually undeformed (Fig. 1a). The second clast fraction comprises pebbles whose longest dimensions vary from 3 to 15 cm, spaced some 10 to 25 cm apart (Fig. 1b). These smaller clasts are dominantly quartzite or psammite (or more rarely, vein quartz or granite) and are more obviously deformed than the larger clast set. We have attempted to analyse the strain in both clast sets, as given in Section 5.2.

The clasts are suspended in a fairly uniform cleaved matrix, which comprises sand- to silt-sized quartz and feldspar grains (0.3–2 mm) that are contained in an even finer matrix ground-mass of white mica and quartz grains (<0.3 mm), as shown in Fig. 1c and d. We estimate an approximate 20% fraction of the coarser matrix grains. There is a well-developed cleavage throughout the matrix, which dips 34° ENE. The deformed pebble-sized clasts are flattened in the cleavage, as detailed below, and are elongated parallel to a strong lineation in the matrix that pitches ~12° S. The quarry-side exposures used for analysis (Fig. 1a and b) are approximately perpendicular to the cleavage and parallel to the lineation, and so are taken as the XZ principal plane of bulk strain (taking ellipsoid axes $X \geq Y \geq Z$). Many clasts have pressure shadows parallel to this lineation, and the quartzite clasts are especially characterised by envelopes of pink dolomite (Fig. 1b). Bedding is locally indicated by strings of psammite, which dip at a steeper angle (e.g. 60°) east than cleavage, the formation here being overturned on the NW limb of the regional Islay Anticline (Bailey, 1917).

5.2. R_f-ϕ analyses of clasts and grains

It is apparent from the rock description, above, that any R_f-ϕ analysis performed on the boulder/cobble or pebble clast fractions cannot be expected to provide a sensible measure of the whole-rock strain. Collectively, these clasts represent only ~10% of the rock area or volume, and so their R_f-ϕ analyses will only reveal part of the strain in the conglomerate. The obvious coarse grains revealed in matrix micrographs are suitable for R_f-ϕ analysis, but the strain deduced from this is not necessarily the same as the whole matrix strain.

Our largest scale of R_f-ϕ analysis addresses the boulder- to cobble-sized clast fraction (e.g. Fig. 1a), using a collection of *field photographs* covering ~10 m^2 of exposure subparallel to the XZ plane. As shown in Fig. 2a, the clasts are grouped as either granites or psammites. We take the mean of their R_f values as the best determination for the average strain for each clast family. The different types of means (arithmetic, geometric, harmonic, and square root of maximum × minumum) are compared in Table 2a, and (as discussed earlier) we will use the harmonic mean in subsequent calculations. In Fig. 2a, we determine mean XZ strain ratios of $R \cong 1.4$ for granite and $R \cong 1.6$ for psammite, which reveal very small strains for both rock types. Because of the size and isolation of these boulders, we do not have large data sets for either rock type, and so cannot be sure of the accuracy of these strain determinations. Nevertheless, our field observations show strong curvature of the rock matrix fabric around the boulders, indicative of heterogeneous strain and a large competence contrast.

At the next scale, we have R_f-ϕ analyses of the smaller pebble-sized clast fraction, as illustrated in Fig. 1b. This and another adjacent photograph have been used, and all visible

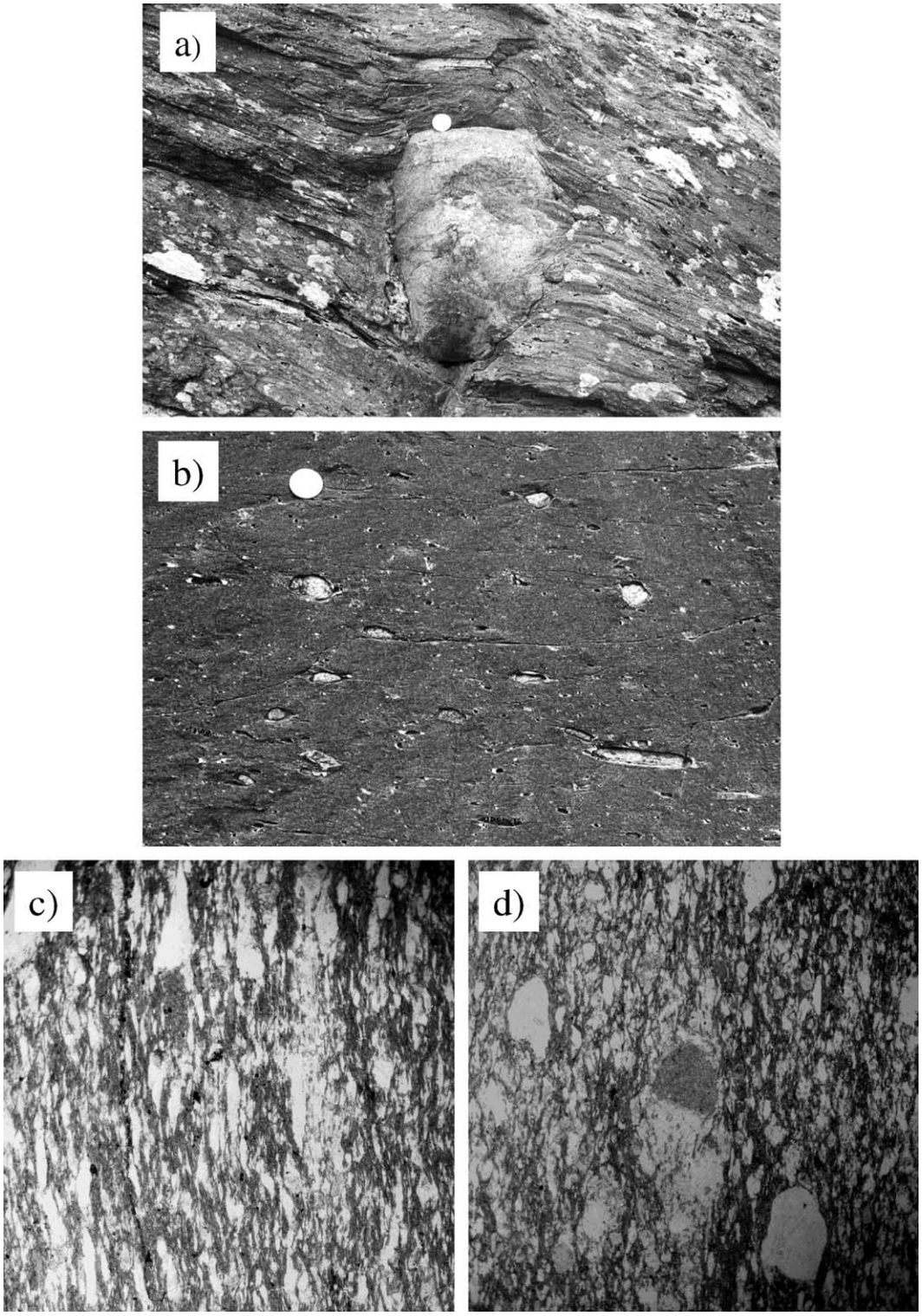

Fig. 1. The Port Askaig Tillite at Scarabus, Islay. (a, b) Field exposures in ~*XZ* sectional view, with 2.5 cm coin (tilted) for scale. (a) Single granite boulder in the matrix, with curvature of the matrix schistosity around it indicating a strong competence contrast. (b) The smaller pebble clast fraction (dominantly fine cream quartzite) dispersed in the grey tillite matrix, with quartz pressure shadows appearing white. (c, d) Photomicrographs of the matrix in plane polarised light, each image 1 cm wide: (c) sectioned perpendicular to schistosity and parallel to lineation (*XZ* section); (d) sectioned perpendicular to schistosity and lineation (*YZ* section). See text for further descriptions.

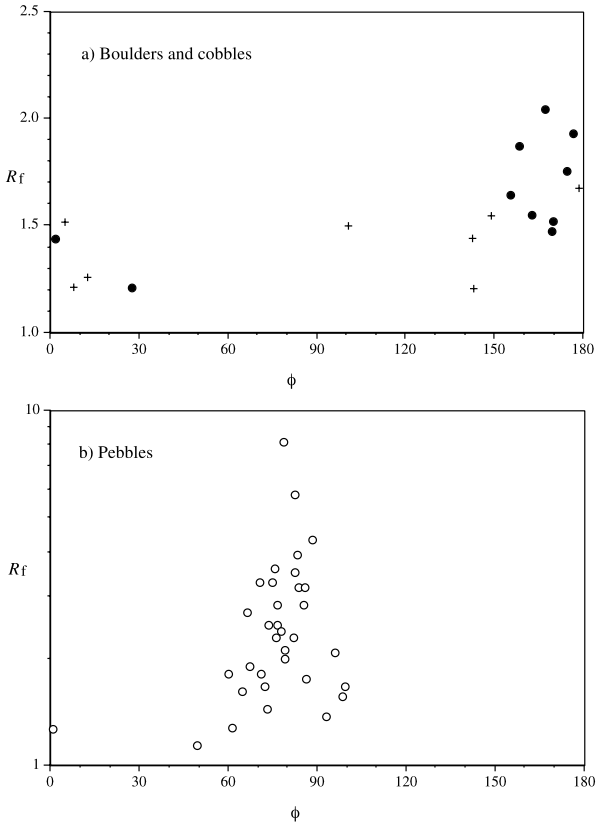

Fig. 2. R_f-ϕ analyses of clasts from photographs of the Port Askaig Tillite. (a) Boulders and cobbles, such as shown in Fig. 1a, with R_f on a linear scale (because R_f values are small); crosses are granites, and solid spots psammites. (b) Pebbles from Fig. 1b and an adjacent photograph, with R_f on usual log scale. See Table 2a for further information and mean values.

and measurable clasts have been analysed over an area of $\sim$0.2 m^2. The clasts are dominantly fine-grained quartzites, but include some psammites. In Table 2b, again we compare the different determinations of mean strain, and derive a harmonic mean of $R = 2.2$ for this clast set. This is a greater strain than derived for the psammite boulders, and the field appearance of these dominantly quartzite clasts also indicates that the competence contrast with the matrix is not so great. We consider the strain difference relates to rock type more than to clast size difference. If the average strain ratio of $R = 2.2$ found here for 'all clasts' is assumed to incorporate a range of competence, encompassing the most competent psammites clasts (with $R \cong 1.6$) and a 'softer' quartzite, we might expect this latter rock type to record strain with $R > 2.2$: perhaps nearer to 3, as suggested by the spread of points in Fig. 2b. This will be examined further in our next type of R_f-ϕ analysis: that of rock specimens.

Rock samples were cut perpendicular to schistosity, and parallel or perpendicular to lineation, providing us with strain measurements on *XZ* and *YZ* principal planes, and thus three dimensions. The R_f-ϕ analyses of small clasts in the tillite matrix are shown collectively in Fig. 3, and further details and mean values are given in Table 2b. These clasts are principally fine-grained quartzite, as described above, but on a slightly smaller scale, and make up 5–10% in *XZ* sections of rock samples. From the harmonic means of *R* for the *XZ* and *YZ* sections, we deduce a triple strain ratio for this clast fraction of approximately 3:2:1. There is evidence in these samples of competence contrast between the measured clasts and the surrounding rock matrix, and so this triple strain is underestimating the whole-rock strain: by how much we try to assess later.

Our smallest scale of R_f-ϕ analysis concerns sand- to silt-sized grains in the rock matrix, using *thin section photographs* (Fig. 1c and d). Imaged at this scale, this gritty matrix has the appearance of a fine breccia or conglomerate: i.e. it comprises a measurable 'clast fraction' ($\sim$20% by area) of generally quite angular grains, suspended in a finer ground-mass fraction. These grains comprise (in order of decreasing frequency) single quartz (0.3–0.6 mm), and notably larger (0.6–2 mm) multiple quartzes or quartzite, single feldspar grains, and composite feldspar/quartz grains. We made R_f-ϕ analyses of these grains in order to obtain a strain for these grains, collectively for the two principal sections (Fig. 4). The statistics and mean values from these R_f-ϕ analyses are given in Table 2c. Using the harmonic means, we obtain a triple strain ratio of 3:2.1:1 for all grains. This is close to the values found for 'all clasts' in hand specimens (Table 2b). These grains make up only about 20% of the matrix, so again it cannot be assumed that their strain is representative of the whole strain in the matrix, or the whole strain in the tillite.

In addition to considering the grains, collectively, we have also attempted to assess the grain strain in terms of their mineralogy, based on 10 grains of three main types: single quartz, quartzite, and feldspar (Table 2c). Despite limitations on these statistics, differences in strain emerge, with feldspar deforming the least, and quartzite the most.

5.3. Matrix or whole rock strain: Fry analysis on two scales

So far, we have unravelled different components and strains in the rock, but only by analysing clast strains from boulder to sand-grain size, using R_f-ϕ analysis. We have discussed in Section 4 the difficulties of obtaining an independent measure of the bulk strain for conglomerates, or indeed for any rock. Here, we follow procedure introduced earlier, by applying Fry analysis on two different scales.

Fig. 5a shows the results of Fry analysis of the *field photograph* shown in Fig. 1b, with parallel figure alignment for convenience. The analysis of clast centres is based on using the same pebble fraction that was used for R_f-ϕ analysis in Fig. 2b, and so is based on the assumption that the clasts and their centres were originally homogeneously distributed, on this scale of the rock. We employed the automated method of Fry analysis outlined in Section 4.

Table 2
Results for Port Askaig Tillite, Scarabus.

(a) R_f-ϕ analyses of field photographs of ~XZ surfaces. Comparison of different calculated mean values: MM is ($R_{fmax} \times R_{fmin}$), AM is arithmetic mean, GM is geometric mean, HM is harmonic mean (used to 1dp for calculations).

Type of analysis	R_f-ϕ diagram	No. of pts	MM	AM	GM	HM
Psammite boulders and cobbles (3–35 cm)	Fig. 2a—spots	10	1.58	1.64	1.63	1.61
Granite boulders and cobbles (e.g. Fig. 1a) (3–35 cm)	Fig. 2a—crosses	8	1.42	1.42	1.41	1.39
All small clasts in ~0.2 m^2 exposure (Fig. 1b) (1–10 cm).	Fig. 2b—all	34	3.05	2.62	2.36	2.2

(b) R_f-ϕ analyses of hand specimens, sectioned perpendicular to cleavage, and parallel to lineation (*XZ* section) or perpendicular to lineation (*YZ* section). Comparison of different calculated mean values, as abbreviated in (a).

Type of analysis	R_f-ϕ diagram	No. of pts	MM	AM	GM	HM
XZ sections of specimens. All measurable clasts (3 mm–3 cm)	Fig. 3a	15	3.18	3.29	3.19	3.03
YZ sections of specimens. All measurable clasts (3 mm–3 cm)	Fig. 3b	31	2.06	2.14	2.05	1.99

(c) R_f-ϕ analyses of grains from thin sections of rock matrix, cut from the same rock samples as analysed in (b). Comparison of different calculated mean values, as abbreviated in (a).

Type of analysis	R_f-ϕ diagram	No. of pts	MM	AM	GM	HM
XZ thin section of matrix (6 mm square from Fig. 1c)						
All measurable grains (0.3–2 mm)	Fig. 4a	128	3.7	3.58	3.32	3.04
Clasts by type:						
Feldspar		10	2.15	2.29	2.25	2.22
Single quartz		10	3.56	3.43	3.35	3.33
Quartzite		10	3.03	3.22	3.16	3.03
YZ thin section of matrix (6 mm square from Fig. 1d						
All measurable grains (0.3–2 mm)	Fig. 4b	178	2.3	2.36	2.23	2.11
Clasts by type:						
Feldspar		10	1.65	1.78	1.75	1.72
Single quartz		10	2.73	2.59	2.56	2.56
Quartzite		10	1.76	1.85	1.82	1.79

(d) Results of Fry analyses of rock or matrix strain (Fig. 5).

Type of analysis	Section	Fry diagram	No of pts	R_S value
'Whole rock' from field photograph (Fig. 1b)	*XZ*	Fig. 5a	28	4.77
Matrix from thin section photograph (Fig. 1c)	*XZ*	Fig. 5b	85	4.78
Matrix from thin section photograph (Fig. 1d)	*YZ*	Fig. 5c	66	2.58

(e) Summary of rheological analysis in (a)–(d), and calculations of viscosity ratios (Eq. (2)), using data for *XZ* sections

Clast or rock type	Approx. fraction, α	Triple strain ratio, or *X*/*Z*	Calculations of principal axes (no volume change)			Viscosity ratio *r* (to whole rock or matrix)
			X	*Y*	*Z*	
Whole rock breakdown						
Whole rock ≅	1					
Matrix	0.9	4.8:2.6:1	2.1	1.1	0.43	1
Granite boulders	~ 0.02	1.4				10.2
Psammite boulders	~ 0.03	1.6				6.8
Quartzite and psammite pebbles—exposure	~ 0.05	2.2				3.5
Quartzite pebbles—specimens	~ 0.05–0.1	3:2:1	1.7	1.1	0.55	2.1
Matrix breakdown						
'All' clasts in matrix thin section: quartz or felspar	0.2	3:2:1	1.7	1.1	0.55	2.1
Remaining (semi-pelitic) fraction: calculated	0.8	5.4:2.8:1	2.2	1.1	0.4	0.83
Matrix clasts/grain type:						
Feldspar		2.2:1.7:1	1.4	1.1	0.64	3.5
Quartzite		3.3:2.6:1	1.6	1.3	0.49	1.8
Single quartz		3:1.8:1	1.7	1.03	0.57	2.1

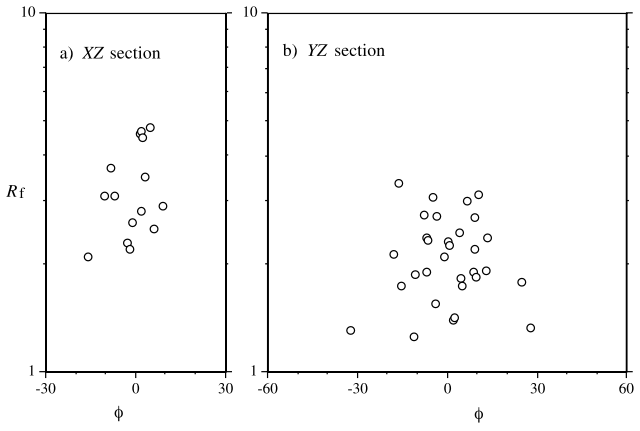

Fig. 3. R_f-ϕ analyses of clasts (quartzite and psammite) from hand specimens of Port Askaig Tillite, cut in (a) *XZ* and (b) *YZ* sections. See Table 2b for further details.

As discussed there, a strong halo of points is not revealed in Fig. 5a, but a good ellipse fit to the innermost points can be found, that has its long axis parallel to the macroscopic cleavage trace in Fig. 1b. This best strain result gives $R \cong 4.8$, and we therefore take this strain value to be a reasonable estimate of the whole-rock strain (in *XZ* section) for the region of this photograph: a considerably higher value than any determined by R_f-ϕ analysis.

In Fig. 5b and c, we illustrate the results of Fry analyses of the two *photomicrograph* images of the rock matrix (Fig. 1b and c). The centres of the white clasts (those measured for R_f-ϕ analysis; Fig. 4) are used in each case. We use the same procedures as above for finding best-fit ellipses. In this case we can derive a three-dimensional strain (Table 2d), an approximate triple strain ratio of 4.8:2.6:1. We note the similarity of the first number to the *XZ* ratio determined in Fig. 5a from the field photograph. This suggests that the strain in the matrix is approximately the same as in the rock on a two orders-of-magnitude greater linear scale, and may therefore be taken as an approximate measure of the microscopic to mesoscopic whole-rock strain. We will therefore use this triple strain ratio as the best available measurement for the matrix and whole-rock strain of the tillite, with the exception of regions of heterogeneous deformation close to the isolated competent boulders.

5.4. Rheology of the Port Askaig Tillite at Scarabus: conclusions

This rock might not be considered an ideal example of a deformed conglomerate, but tillites and diamictites probably provide the best geological examples of weak suspensions of clasts in a matrix, as discussed theoretically in Section 3. This example is especially interesting, as it affords at least three distinct scales of analysis, each revealing a type of clast–matrix suspension or mixture. First, at the largest scale (Fig. 1a), we have an approximate 5%

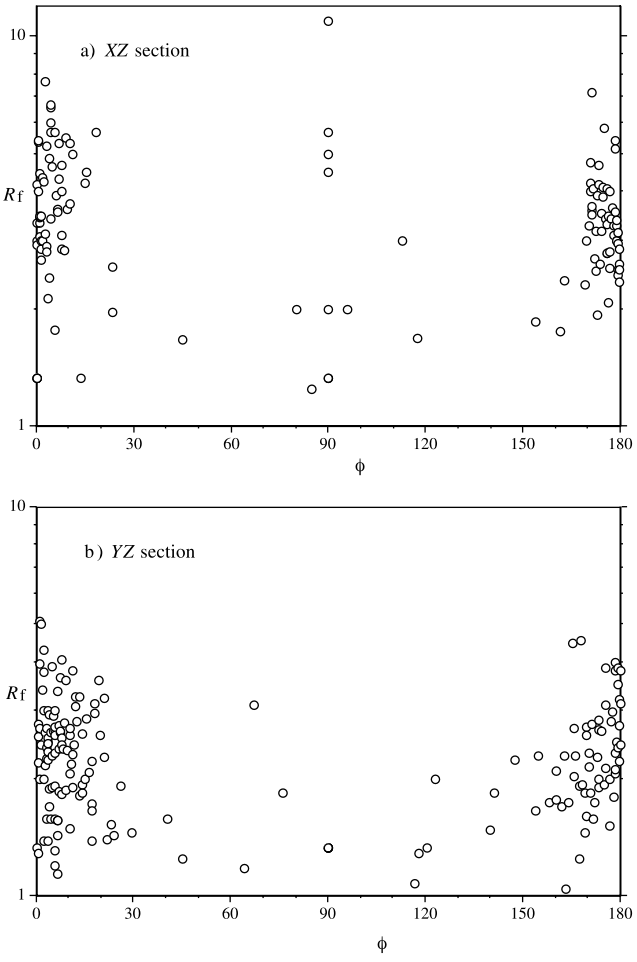

Fig. 4. R_f-ϕ analyses of grains in the matrix in (a) *XZ* and (b) *YZ* section, measured from Fig. 1c and d, respectively. See Table 2c for further details.

fraction ($\alpha = 0.05$) of isolated boulders of granite or psammite, that are only very slightly deformed, suspended in the tillite ground mass. Secondly, this ground-mass itself contains about 5% fraction of smaller pebble-sized clasts (Fig. 1b), which are dominantly a finer quartzite that is more measurably deformed, which are suspended in the main gritty matrix. Thirdly, this gritty tillite matrix contains about 20% of quartz or feldspar grains, in an even finer semipelitic type of matrix (Fig. 1c). On the basis of proportions alone, it is clear that R_f-ϕ analysis of the clast fractions of a rock of this kind is a poor method for estimating the bulk strain, unless there is no obvious competence contrast among clasts and matrix.

From modelling of mixtures in Appendix B (e.g. Fig. B1), it would be deduced that a two phase mixture with very small competent fraction ($\alpha_2 < 0.1$), which we suggest is the boulder to pebble fraction in this rock, would have a bulk viscosity only marginally greater than the matrix viscosity. We have not yet quantified the viscosity ratios of the boulder or pebble fractions, with respect to the matrix or whole rock. If these clasts were modelled together as *one average competent phase*, with $\alpha_2 = 0.1$, and with a

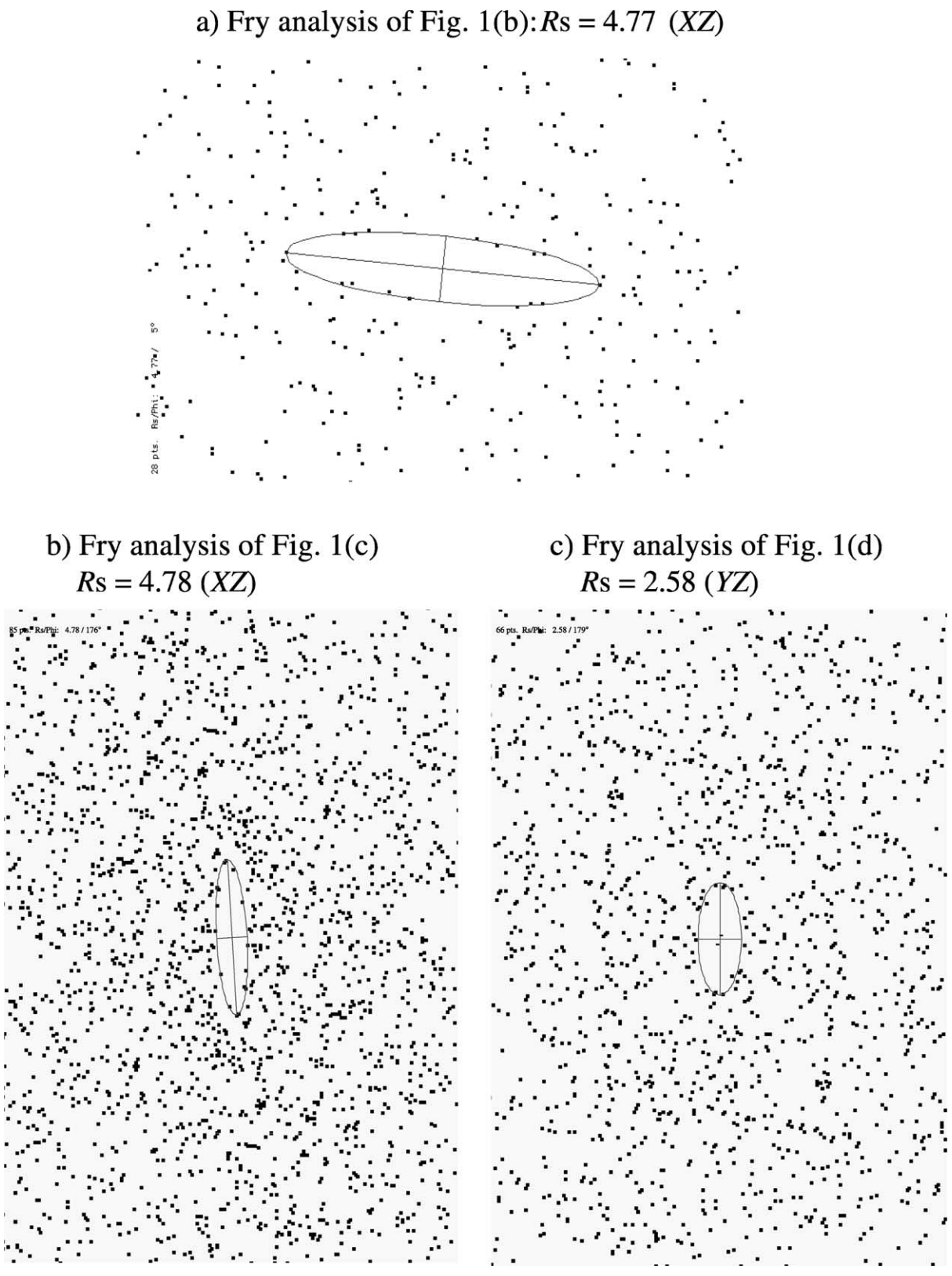

Fig. 5. Fry analyses of the Port Askaig Tillite. (a) Analysis of field photograph (Fig. 1b), similarly oriented, using centres of the pebble-sized clasts; the comparable R_f-ϕ analyses are shown in Fig. 2b. (b) and (c) Analyses of thin sections (Fig. 1c and d) using centres of white grains; the comparable R_f-ϕ analyses are shown in Fig. 4. The best-fit strain ellipses are outlined on each figure, and their R_S values are shown, and also summarised in Table 2d.

viscosity ratio to the matrix of 10 (which is as great as might be expected; see Table 1), the bulk viscosity relative to matrix viscosity would be found to be $\beta = 1.2$. If we now break this down into the two size fractions, it would be equivalent to stating that for each different 0.05 fraction (boulders, pebbles) there would be a $\times 1.1$ change in viscosity with each fraction: from the matrix to hand specimen; and from the hand specimen to the exposure scale. The same degree of small change is found from using Fig. B3, here with an $\alpha_1 = 0.9$ matrix fraction and equal fractions of two different competent clasts ($\alpha_2 = \alpha_3 = 0.05$).

Thus, as a first order analysis, we conclude that the whole rock strain and the matrix strain are virtually the same, and that the triple strain ratio (4.8:2.6:1) deduced from Fry analysis on two scales is the bulk strain in this tillite. Assuming no volume change, these values convert to bulk stretches of $X = 2.1$, $Y = 1.1$ and $Z = 0.43$ (Table 2e). This is almost plane strain, a fortunate finding that legitimises use of theory and modelling of clast–matrix systems based on two-dimensional analyses and approximations. These strain values can be compared with calculations made by Borradaile and Johnson (1973), using deformed sedimentary dykelets in the adjacent Dolomite Formation of the SE limb of the Islay Anticline at Bonahaven, 10 km away. For three localities, they determined X values of 2.1–2.4, Y of 0.9–1.3, and Z of 0.3–0.5.

We deduce a weaker strain in the medium-sized quartzite clasts, with triple ratio of 3:2:1, and approximately the same value for smaller grains in the matrix. This translates into $X = 1.7$, $Y = 1.1$ and $Z = 0.55$, again close to plane strain. This tillite thus deformed in approximate plane strain, with 45% shortening affecting the pebble clast fraction, and 57% affecting the matrix and the whole-rock scales. We calculate in Table 2e that to account for the difference in these strains, there needs to be a greater deformation in the unmeasured finest semipelitic part of the rock matrix. Using Eq. (3) for the 'weighted strain' in terms of $\ln R$ values and α fractions, we would need a triple strain ratio of 5.4:2.8:1 in this semipelitic remnant, giving $X = 2.2$, $Y = 1.1$ and $Z = 0.4$.

On the basis of the above values derived for the bulk strain, we can now compute the viscosity ratios of the different clast rock types, relative to the whole rock (or matrix), using Eq. (2) or Fig. A1. These calculations, and the results shown in Table 2e, concern only the XZ strain ratios, using the bulk strain of $R_S = 4.8$. As anticipated from Fig. 2a, the highest viscosity ratio ($r \cong 10$) is found for granite boulders, and values ranging from $r \cong 7$ for psammite boulders, to $r \cong 2$ for fine-grained quartzite clasts. At the smallest scale of measurable grains in matrix, we estimate that feldspar is the stiffest ($r = 3.5$) and 'quartzite' grains the least stiff ($r = 1.8$), almost a two-fold difference. The semipelitic remainder of the matrix, as extrapolated above, would have a viscosity ratio of 0.83 relative to the rock. This is not a large contrast, but appears broadly consistent with measurements in other studies (Table 1) as well as our next example.

In conclusion, despite the obvious competence contrasts between clasts and matrix exhibited by this rock in the field, and in the strain variations, we deduce the maximum viscosity contrast among all the measured rock components of only one order of magnitude (granite to matrix). By indirect calculations, we calibrate the viscosity contrasts relative to semipelite to be ~12 for granite, and in the range of 7.6 to 2.5 for psammites to quartzites.

6. Cesson Conglomerate, Brittany, France

6.1. Introduction and rock description

This second example is a strongly deformed conglomerate that contains closely packed clasts of a variety of rock types (Fig. 6). It therefore provides a good case study for a complex multiphase mixture, at the other end of the spectrum from the preceding tillite case study. Our data for this conglomerate study were collected from La Pointe du Nord and La Petite Grève, 2 km SE of the village of Cesson, near St Brieuc, northern Brittany. (Map and further details available from the authors.) According to Roach et al. (1986), the outcrop is part of the Cesson Conglomerate Member of the Hillion Volcanic Formation, near the base of the Brioverian succession, which here immediately overlies blastomylonites of the Pentevrian basement. The rocks have been deformed in the Cadomian Orogeny (?late Proterozoic) and affected by upper greenschist to lower amphibolite grade metamorphism.

From its field and specimen appearance (Fig. 6), this rock is a clast-supported conglomerate, with a population of distinct fairly rounded clasts of granites, volcanics or psammite, perhaps constituting 30% volume. These are set in a darker groundmass that comprises pebbles and rock fragments of these lithologies, but more dominantly of psammite to semipelite, on a decreasing scale that blurs into the indeterminate matrix. The clasts are clearly flattened in the dominant schistosity, which, together with the sub-parallel bedding, dips steeply ~86° N, and are elongate parallel to a strong linear fabric in the matrix, that pitches ~75° E on the schistosity planes. Clasts of different lithologies are deformed to different extents, as quantified below, but the longest dimension of the most abundant clasts (various fine-grained volcanic rocks, coarse-grained granitoids, psammites and semipelites) varies from 2 to 10 cm. Most of the distinct clasts in Fig. 6 fall into the 20–40 cm size range, but exceptional large clasts of granite with longest dimensions of 125–140 cm locally occur.

At this coastal locality, the best surfaces for analysis, directly in the field or via photography, are wave-polished subhorizontal exposures subparallel to the macroscopic YZ principal surface (e.g. Fig. 6b). Surfaces parallel to

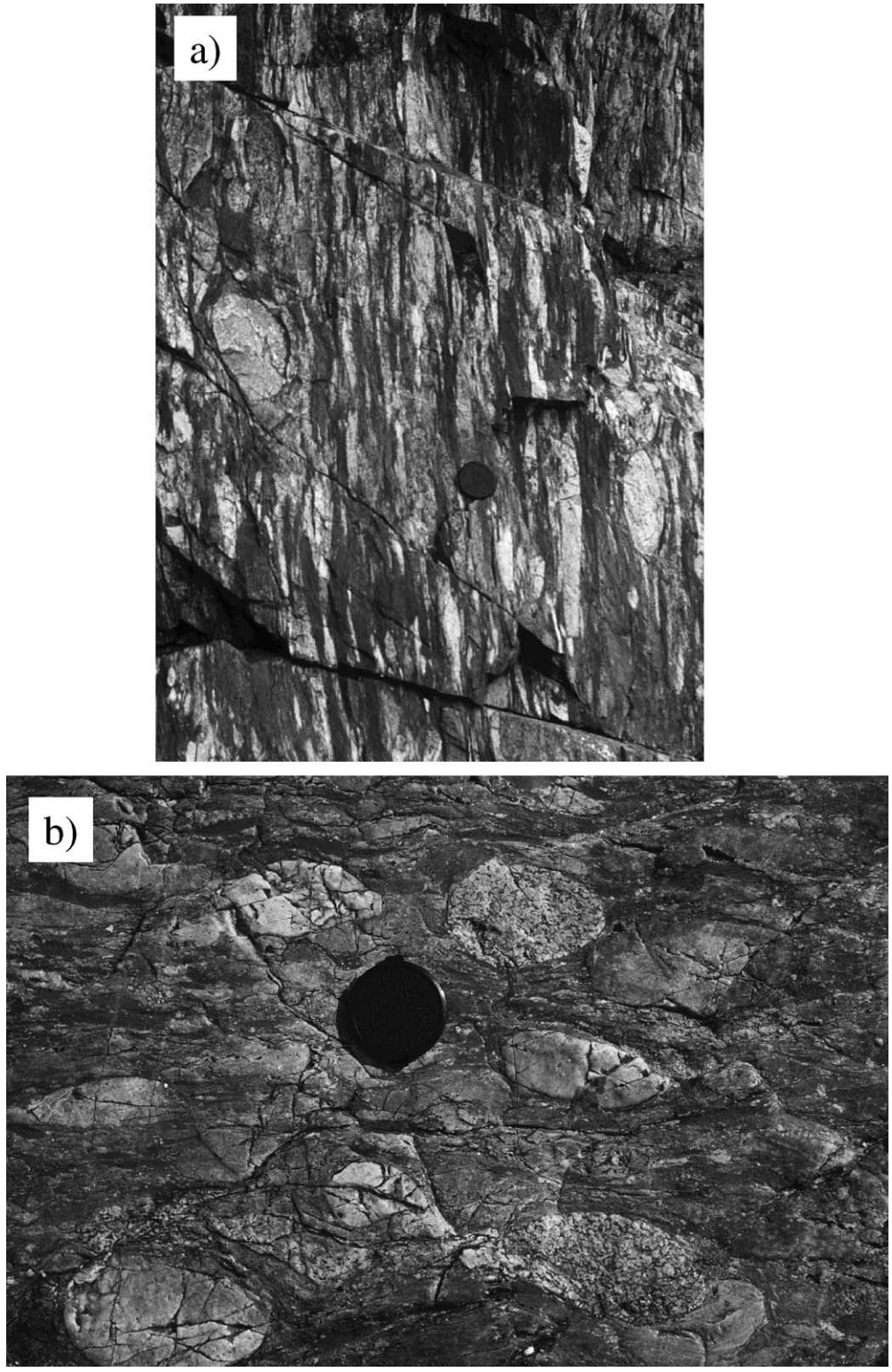

Fig. 6. The Cesson Conglomerate from Brittany. (a) Field exposure in subvertical section approximately parallel to *XZ*, showing strong deformation and streaked clasts. (b) Subhorizontal wave-cut exposure, approximately parallel to *YZ*, which more clearly reveals the polymict nature of the conglomerate: e.g. pale fine-grained volcanic clasts and crystalline granitic clasts in a darker 'matrix' that comprises a clast mixture on a smaller scale. 5 cm lens cap for scale, in each.

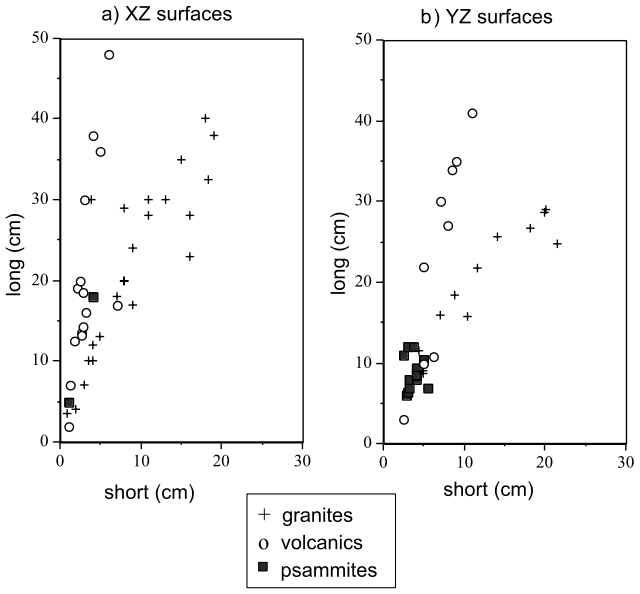

Fig. 7. Field measurements of long and short axes of Cesson Conglomerate boulders and pebbles, in exposures subparallel to (a) *XZ*, and (b) *YZ*. See Table 3a for mean values.

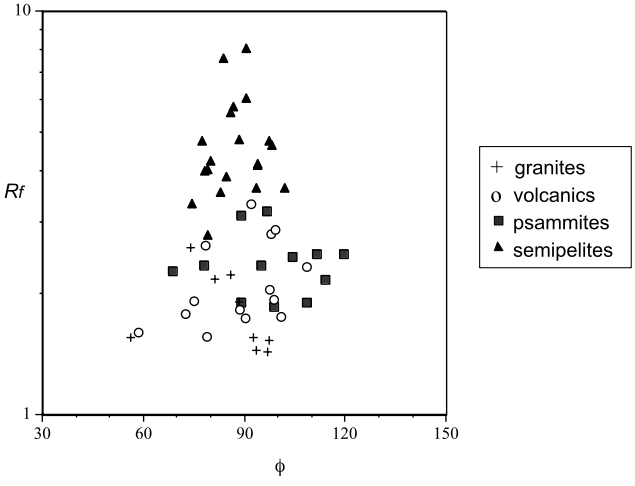

Fig. 8. R_f-ϕ analyses of clasts from photographs of a field station at Cesson that includes Fig. 6b. See Table 3b for details and mean values.

the *XZ* principal plane (subvertical) are less clear in exposure (e.g. Fig. 6a), and it is more difficult to distinguish their rock types and clast outlines for deformation analysis.

The pebble to cobble-sized clasts were classified roughly by field appearance and rock type, as described above, and then more precisely attributed to rock-type groups by subsequent thin-section analysis. This Cesson Conglomerate contains a wide variety of component rock types, so some simplifications are needed when seeking to describe the rock in terms of a finite number of distinct rock phases. Accordingly, we have used four groups to classify the principal clast components and their area fractions: (1) fine-grained or porphyritic rhyolites, rhyodacites and other acid volcanics, whose weathered appearance is cream to pale grey (fraction uncertain; 10% large clasts plus an unknown finer fraction); (2) coarser-grained igneous rocks encompassing granites, granite-gneisses, microgranites or microdiorites (8–10%); and an almost continuous spectrum of clastic rocks, broadly grouped as (3) grey psammites to (4) dark grey semipsammites to semipelites to black pelites, forming the remainder. Unusually for a conglomerate, quartz clasts were rare; clasts considered as quartzite in the field were found from thin section analysis to be largely rhyolites.

What appears to be the 'matrix' to the distinct competent clasts seen from field photographs (Fig. 6a and b), in fact comprises large numbers of less distinct and more highly deformed clasts, as noted above, and seen in cut specimens. It is difficult to distinguish the elongate semipelite clasts from semipelitic matrix, and so for this rock, we cannot quantify a separate true matrix fraction.

6.2. Measurements of clasts, and R_f-ϕ analyses

Our first analyses are *field measurements* of long and short axes of pebble, cobble and boulder clasts, represented in Fig. 7a for 'steep' surfaces (~*XZ*), and in Fig. 7b for 'flat' surfaces (~*YZ*). These measurements concentrated on the igneous clasts that were distinct and easily measurable in outcrop, and were broadly classed as volcanics or granites. Fig. 7 thus reveals the true size ranges of these types of clasts in section, as noted earlier. The few measurements made for grey psammite clasts in *XZ* section reveal the difficulties in distinguishing the clast outlines for this rock type, but the more numerous data in the clearer *YZ* sections suggest a narrower size range for the psammite clasts. If the points for each rock group fall on an approximate straight line, as seems to be the case (especially for the *XZ* measurements), it might be deduced that there is no influence of clast size on strain, and the gradient of the best line fit can be taken as the average rock strain ratio. We use the more precise harmonic mean of all the long/short ratios (as also used for R_f-ϕ data) to determine the mean values for these field-measured data, and the results are listed in Table 3a.

Our next clast analyses come from a collage of *field photographs* of clean subhorizontal (*YZ*) rock exposures (e.g. Fig. 6b), shown in Fig. 8 as an R_f-ϕ graph. The clasts are subdivided into four rock groups, as defined above: volcanics, granite, psammites or semipelites (semipsammite to pelite). Even with this small sample of measurements, the R_f-ϕ data show distinct clusters, according to rock type. The granite, volcanics, and psammite clasts have a range of $R_f = 1.4$ to ~3, whereas the incompetent semipelite clasts, identified in the darker ground-mass, show higher R_f values of ~3 to 8. Further information, and the harmonic mean strain ratio for each set, are given in Table 3b. The mean 'all clasts' strain for this *YZ* section is found to be $R = 2.5$. This value partly depends on the numbers of clasts of each

Table 3
Results for the Cesson Conglomerate

(a) Harmonic means of clast axial ratios measured in the field, for *XZ*- and *YZ*-parallel surfaces, for three clast rock types (see Fig. 7)

Clast rock type	*R* (*XZ*)	Measurements	*R* (*YZ*)	Measurements
Volcanics	5.2	15	2.6	9
Granites	2.4	23	1.7	12
Psammites			2.3	13

(b) Harmonic means *R* values from R_f-ϕ analyses of clast rock types from field photographs in *YZ* sections (see Fig. 8). Note also the area fractions of each rock, used to estimate the 'weighted mean strain' for the rock

Rock type	*R* (*YZ*)	Measurements	Fraction (α)
'All clasts'	2.5	55	(0.30)
Volcanics	2.0	14	0.12
Granite	1.8	9	0.08
Psammite	2.3	12	0.45
Semipelite	4.4	20	0.35
Rock (weighted mean)	$R_S = 2.8$		1.0

(c) Harmonic means *R* values from R_f-ϕ analyses of clast rock types from hand specimens in *YZ* and *XZ* sections (see Fig. 9)

Rock type	*R* (*XZ*)	Measurements	*R* (*YZ*)	Measurements
"All clasts"	5.5	104	2.6	145
Volcanics +	5.2	65	2.3	86
Granites	2.3	6	1.9	17
Semipelite	8.8	23	4.7	32

(d) Fry analyses of 'whole rock' strain, to determine R_S (see Figs. 10 and 11). The mean values given in the last line are used as the best estimate for bulk strain

Analysis type	Section	No. of pts	R_S value	Section	No. of pts	R_S value
Field photographs	*XZ*	41	6.97	*YZ*	42	3.20
	XZ	25	7.62	*YZ*	38	2.89
Hand specimens	*XZ*	29	7.48	*YZ*	50	2.86
	XZ	33	7.34	*YZ*	72	2.94
Mean R_S values	*XZ*		7.3	*YZ*		3

(e) Summary of best mean strains for each rock type, and calculations of viscosity ratios, using *XZ* strains and applying Eq. (2). Weighted mean calculated from Eq. (3), by simplifying the rock to three phases and using best α estimates

Rock type	Fraction (α)	*X:Y:Z*	Calculations of principal axes (no volume change)			Viscosity ratio *r*: (rock/whole)	Viscosity ratio rock/semipelite
			X	*Y*	*Z*		
Whole rock Fry av.	1	7.3:3:1	2.61	1.07	0.36	1	1.3 ($= \beta$)
Volcanics + psammite	~ 0.22	5.2:2.3:1	2.27	1.0	0.44	1.5	1.9
Granite	~ 0.08	2.3:1.8:1	1.43	1.12	0.62	4.5	5.7
Semipelite	~ 0.7	8.8:4.7:1	2.55	1.36	0.29	0.8	1
Weighted mean using α	1.0	$X/Z = 7.0$					

type that were recognised and measured, and their proportions cannot necessarily be assumed to be a reliable indicator of the true fractions of these rock components in the whole conglomerate.

From this field exposure of a *YZ* section, the distinct pebble/cobble clast fraction of largely competent rock types occupies about 0.3 fraction, roughly comprising 0.12 of volcanics, 0.1 psammites and 0.8 granites. The remaining 0.7 ground-mass fraction appears to be a mixture of smaller clasts of the above types, together with more abundant grey to dark grey clasts or matrix material, and the average lithological composition appears to be a mixture of semipsammite, semipelite and pelite. If these fractions (summarised in Table 3b) are used to derive a weighted mean strain (applying Eq. (3)), we deduce a mean rock strain of $R_S = 2.8$. These fractions are only approximate, and are based on using areas in *YZ* sections (rather than the preferred *XZ*). Variations of

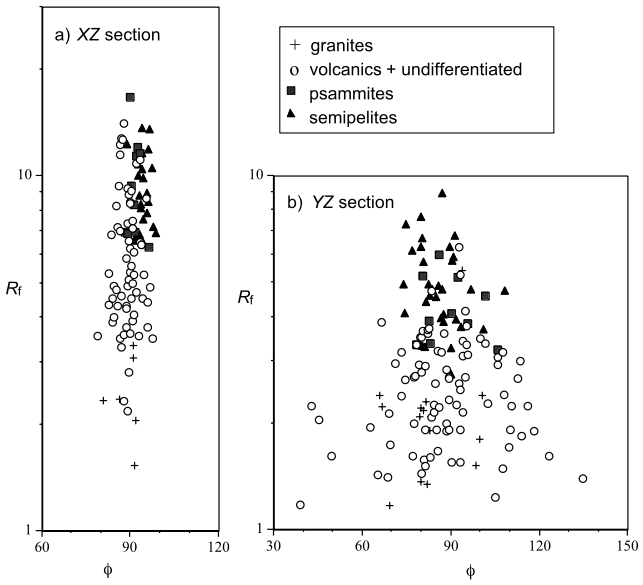

Fig. 9. R_f-ϕ analyses of clasts traced from sections of two hand specimens of the Cesson Conglomerate, 10×15 to 10×20 cm^2 in section size, cut (a) parallel to *XZ* and (b) parallel to *YZ*. See Table 3c for further details.

± 0.1 in the relative fractions of psammite and semipelite yield differences in R_S of ± 0.2.

Our third category of clast analyses concerns *hand specimens*, and R_f-ϕ analyses of identifiable clasts in orthogonal *XZ* and *YZ* sections, which produce measurements of three-dimensional strain. We have identified four classes of rock clasts similar to those used for field-based analysis; but because these analyses include clasts on a smaller scale (long axes mainly in the 0.5 to ~6 cm range), identification was not always easy, and so the rock classes may be somewhat overlapping. There is no obvious boundary between the classes of grey semipsammite, dark grey semipelite and black pelite, rather a sliding scale. The subdivisions were particularly difficult in *XZ* sections.

These R_f-ϕ diagrams (Fig. 9) again clearly indicate different degrees of average strain among the four different rock types (cf. Fig. 8). Harmonic mean *R* values have been computed for all the clasts collectively, and for the main rock groups in Table 3c. The small number of data points for clasts grouped as granites and psammite might cast doubt on the validity of obtaining mean strains for these rock types. However, the statistics for volcanic clasts are better, and we are confident in deducing an average triple strain ratio of 5.2:2.3:1 for this group. Assuming no volume change, this gives stretch values of $X = 2.3$, $Y = 1.0$ and $Z = 0.44$, almost exact plane strain. Because of the similarity in values and harmonic means for the semipsammites, semipelite and pelites, we group them collectively as 'semipelites' in Table 3c, and in later calculations.

The 'all clasts' strain gives a triple strain ratio of 5.5:2.6:1, which translates into a strain ellipsoid of $X = 2.3$, $Y = 1.1$ and $Z = 0.41$. This is quite close to the value for the volcanic clasts. It is a slightly greater 'all clasts' strain than was determined from measurements of the long/short axes of clasts in the field, because the 'all clasts' in our rock specimens include a proportion of small semi-pelite clasts that were not distinguishable from 'matrix' in outcrop.

6.3. Fry analyses to determine whole-rock strain

Following the procedures described earlier, we have made Fry analyses both of field photographs and of cut rock samples. Fig. 10 shows results from analysis of *field photographs* for two different *XZ* surfaces (a, b) (e.g. Fig. 6a), and two *YZ* surfaces (c, d) (e.g. Fig. 6b). These again illustrate that the Fry method for conglomerates does not usually produce a strong halo, but a diffuse vacancy in which to fit a 'best ellipse' to be taken as the bulk strain ellipse, with axial ratio R_S. For each of the four diagrams, we have aligned these Fry ellipses with their long axes sub-parallel to the macroscopic fabric trace in the source slides or photographs; and then by eye have aimed to find the one that approximates or touches the maximum number of innermost points. The computer-based method we used is interactive, and experience with many 'tries' shows that the results may be quite subjective, with small variations in the chosen criteria sometimes yielding significant differences in *R* value. Fig. 10 presents the best result of many tries. The resulting R_S values are listed in Table 3d, and are seen to give a triple strain ratio of 7–7.6:2.9–3.0:1. The poorer results (and number of points) for *XZ* outcrop surfaces reflect difficulty both in finding good field sections in this orientation, and in identification of clasts and their centres because of the extreme deformation.

Fry analyses of *hand specimens* sectioned perpendicular to cleavage and parallel to stretching lineation (two *XZ* sections), and perpendicular to cleavage and to lineation (two *YZ* sections), are shown in Fig. 11. The cut surfaces were scanned, and the Fry analyses are based on centres of the same clasts used for R_f-ϕ analysis in Fig. 9. As noted above, the results and ellipse fitting were easier for the *YZ* sections ($R_S \cong 2.9$), than for the more intensely deformed *XZ* sections ($R_S = 7.3$ to 7.5), and the data are summarised in Table 3d.

Given some questions of precision in these Fry analyses, especially for *XZ* sections, we consider it best to combine the results of the photograph and hand specimen analyses (Figs. B1 and 15), to determine the *mean* R_S values for each principal section (see Table 3d). While it might not necessarily have been assumed that the results would be the same for strain on these two different scales, their value ranges suggest that this is the case. Accordingly, we take the mean values of $R_S = 7.3$ for the *XZ* sections, and $R_S = 3.0$ for *YZ*. These yield the 'whole rock' triple strain ratio of 7.3:3:1, which (assuming no volume change) represents a strain ellipsoid with $X = 2.6$, $Y = 1.1$, and $Z = 0.36$, again close to plane strain. We are not aware of any other studies of

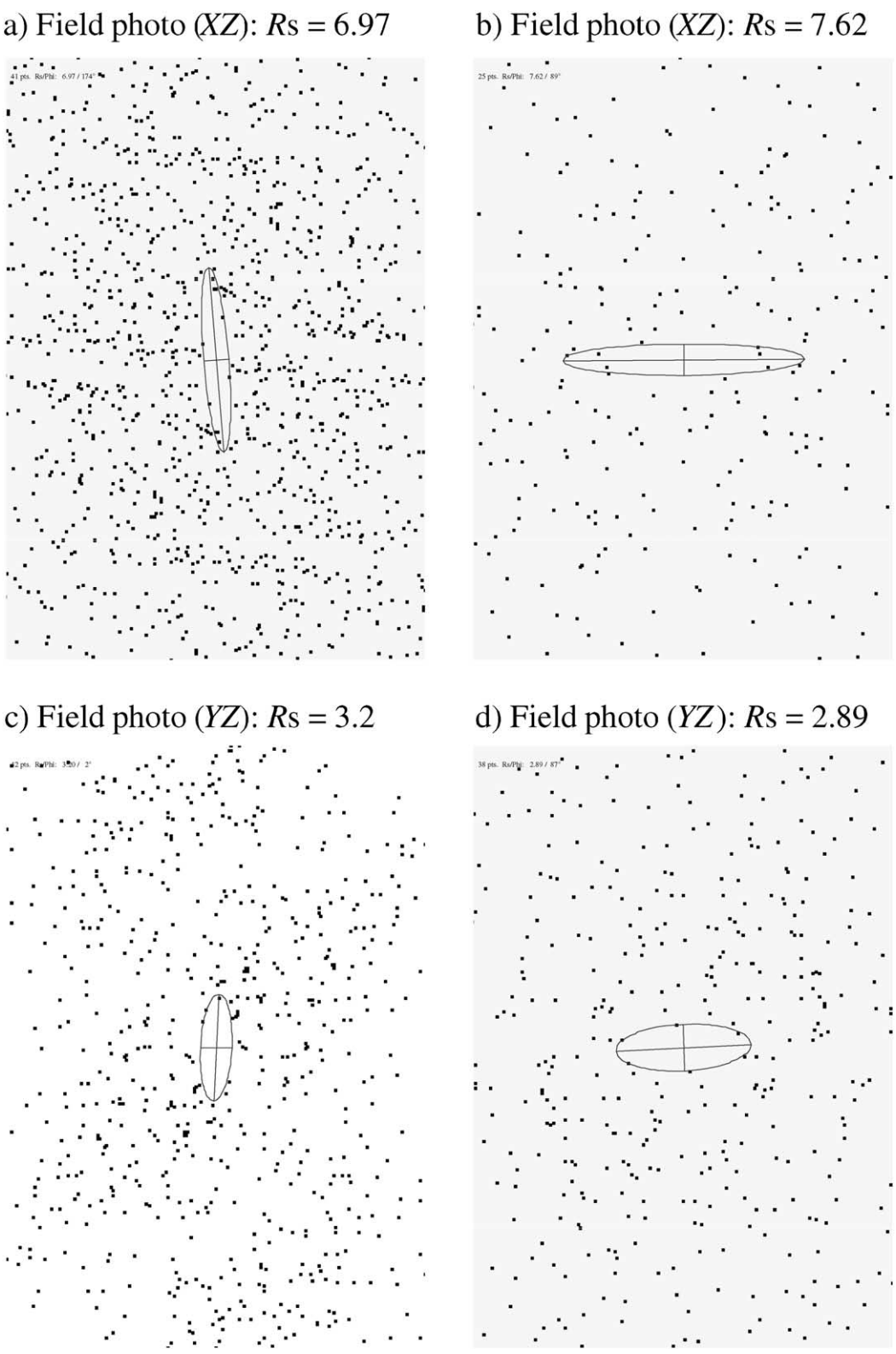

Fig. 10. Fry analyses of the Cesson Conglomerate from two different field photographs of *XZ* surfaces (a, b) and *YZ* surfaces (c, d), using all distinguishable clasts. The best-fit ellipses are outlined on each figure, and the R_S results shown. Differences in orientation (orthogonally) between diagram pairs are not significant, but reflect scanning directions. Further details in Table 3d.

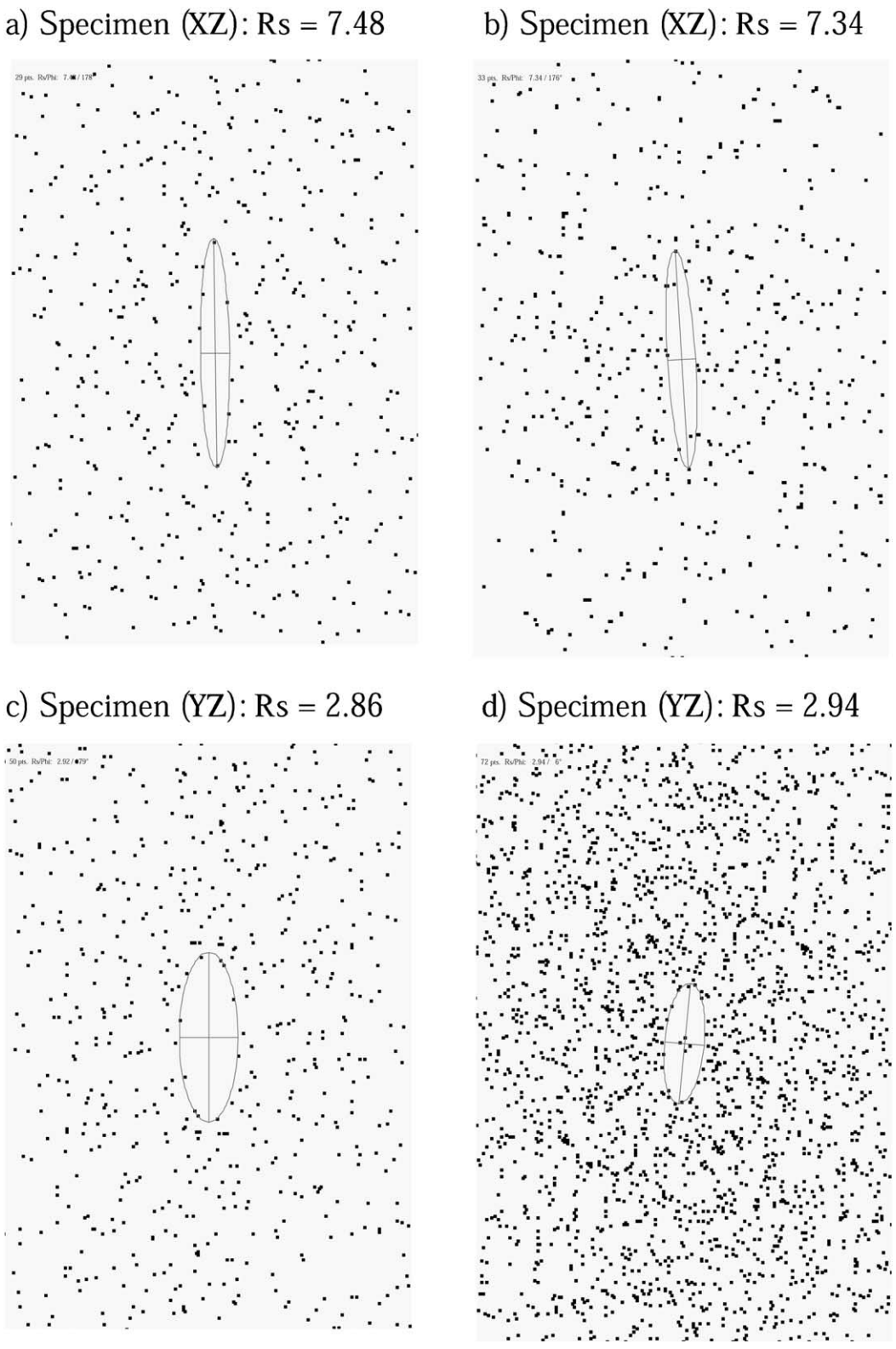

Fig. 11. Fry analyses from sections of two hand specimens of the Cesson Conglomerate, using scans of two serial sections of each, 10×15 to 10×20 cm^2 in size: (a, b) cut parallel to *XZ*; (c, d) cut parallel to *YZ*. Best-fit ellipses are outlined on each figure, and the R_S results shown for each, also in Table 3d.

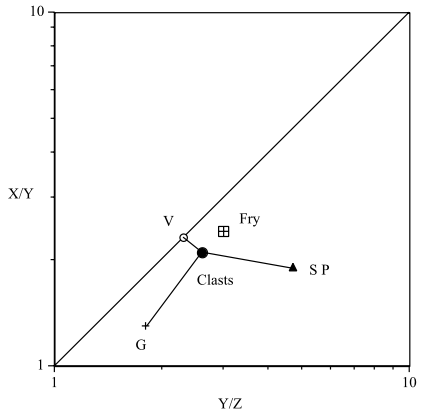

Fig. 12. Flinn graph of *X*/*Y* versus *Y*/*Z* (log scale), using mean strain values for the Cesson Conglomerate given in Table 3. Solid circle represents the mean value for 'all clasts' analysed in hand specimens (Table 3c). Tie-lines to G, V and SP show values for volcanic, granite and semipelite clasts (Table 3e). The quartered square symbol represents the mean whole-rock strain determined from Fry analyses (Table 3d).

strain in these Brioverian rocks with which to compare these results.

6.4. Rheology of the Cesson Conglomerate: conclusions

Our results have shown that the strains determined by R_f-ϕ analysis, for all the pebble-sized clasts or for clasts grouped by rock type, yield different values from those deduced from Fry analysis. Even where efforts are made (as in our analysis of rock samples) to measure all identifiable rock clasts, there is a significant proportion of the rock volume that is omitted from R_f-ϕ analysis: i.e. the finer ground mass or rock matrix, likely to comprise more incompetent rock types than the pebble fraction. Therefore, although R_f-ϕ analysis is the most obvious and popularly used technique for determining strain in conglomerates, it might generally be expected to produce an *underestimate* of the whole rock strain, as suggested in this example. The degree of the underestimate will depend on the viscosity contrasts among the component rock fractions, and on how many 'hidden' clasts of incompetent to average lithology have been sampled, relative to more obvious competent conglomerate pebbles.

For this Cesson Conglomerate example, and assuming no volume change, we determine $X = 2.3$, $Y = 1.1$ and $Z = 0.41$ for 'all clasts' (hand specimens), but $X = 2.6$, $Y = 1.1$, and $Z = 0.36$ for the 'whole rock' strain (specimens and field exposures). The difference appears more significant when comparing the *X*/*Z* ratios of 5.5 and 7.3, respectively. If geologists seek only to obtain very rough estimates of maximum shortening, the differences between 59 and 64% may matter less, especially given the assumptions that underlie both methods of strain analysis.

We combine and summarise the main strain data derived for the different rock types in Table 3e. These values are also represented as a Flinn diagram in Fig. 12. What is interesting about the Flinn plot is that it overemphasises the differences from plane strain. Our listed *Y* values (Table 3e) average about 1.1, and yet when taken with the differences in *X* and *Z*, appear to show significant variations in oblateness of the strain in the different rocks. A degree of differential 'flattening' (i.e. more oblate strain) is definitely suggested for the semipelites ($Y \cong 1.4$), which confirms the expected behaviour of incompetent rock inclusions in bulk plane strain (Freeman and Lisle, 1987). However, it may also reflect that for this family of clasts (originally silty mudstone), the theoretical assumptions of originally random ellipsoidal clasts shapes (i.e. statistically spherical) are not met: or that deformation is associated with volume loss (Ramsay and Wood, 1973). The apparent oblateness of the granite strain, which (after Freeman and Lisle, 1987) might be expected to show a more prolate strain, may simply reflect the results of computing mean strain from a small dataset that may not necessarily represent a statistically random or 'spherical' sample.

The whole-rock strain from Fry analyses is sufficiently close to plane strain for the preceding theoretical modelling of inclusion–matrix systems and rheology of mixtures in plane strain to be applicable. Table 3e summarises the *X*/*Z* strain ratios that we use as *R* values for estimating the viscosity ratios among three distinguishable rock types. In view of the similarity of the results listed in Table 3a–c for volcanic and psammite clasts, and also the difficulties in drawing boundaries between semipsammite, semipelite and pelite noted earlier, we summarise our information (Table 3e) in terms of three rock classes: volcanics with psammite (here apparently rheologically very similar); granite; and semipelite (semipsammite to pelite). Using Eq. (2), we determine viscosity ratios for these rock groups relative to the bulk rock (variable *r*), as given in Table 3e. It is seen that only granites and semipelites have a marked viscosity contrast to the whole rock of $r = 4.5$ and 0.8, respectively. Recalibrating these as viscosity ratios relative to 'semipelite', it is seen that the whole rock is about 1.3 × stiffer than semipelite (this is the physical meaning of the β variable in Appendix B). The volcanic group has almost twice the viscosity of the semipelite. The granites are calculated as almost 6 × more viscous than semipelite, but still within one order of magnitude contrast. These measurements are subject to the *r* value for semipelite being correctly determined, but we found a similar value for the preceding tillite example (Table 2), and this also compares well with values for shale given by Lisle et al. (1983) (Table 1b). All these results together suggest that viscosity contrasts among many common rock types are quite small, but nevertheless result in measurable differences in strain.

In our opening description, we approximated this conglomerate to consist of only four rock types, which makes it analogous to a *four-phase mixture*. Because of the unequal fractions, and unequal changes in viscosity contrasts, the mixture is not found to fit any of the 'equal

fraction, equal factor' three- or four-phase mixtures discussed in Section 3 and Appendix B (Fig. B2). However, if the strain determined for some of the rock types is close enough to group them together as rheologically similar (even though lithologically dissimilar), as suggested above, the rock mixture might be modelled more simply. Accordingly, we can model the Cesson Conglomerate as a *three-phase mixture* of semipelite, volcanics + psammite, and granite (written in terms of increasing competence), with a triple viscosity ratio of 1:1.9:5.7, and α fractions of 0.7, 0.22 and 0.08 (Table 3e). The weighted mean strain (for *X/Z*) for this three-phase mixture, is $R = 7$ (Eq. (3)), which is a slight underestimate of what we determined from the Fry analyses.

At an even cruder level, the rock might be modelled as a *two-phase* clast–matrix suspension, with approximately equal fractions of a 'clast phase' with average 'all clasts' properties, and a 'matrix phase' largely of semipelite. Using the R values in Table 3c and Eq. (2), we determine $r \cong 1.4$ for the clasts and $r \cong 0.8$ for the matrix (the reciprocal of the latter giving us a bulk normalised viscosity for the rock of $\beta \cong 1.3$, as derived in Table 3e), and a two-phase viscosity ratio of $m \cong 1.8$ (cf. Fig. B2a). So in conclusion, this multiphase rock can be modelled, rheologically, as a simple mixture of a few dominant phases, and even perhaps as a two-phase mixture of clasts in a matrix.

7. Conclusions

1. For many years, conglomerates have been regarded as useful rocks for measuring geological strain, and have played an important role in development of techniques of strain analysis. Conglomerates with a variety of clast rock types that show differences in strain (i.e. competence contrasts) may appear less well-suited for use as strain horizons, but have the potential to provide information on viscosity contrasts among the different rock types.
2. The strain determined from R_f-ϕ analysis of all the clasts in a conglomerate is likely to be an underestimate of the whole-rock strain, unless the measurements represent all the component rock types (including matrix), in correct proportion. However, R_f-ϕ analysis can usefully be applied to populations of clasts of similar rock type, in order to determine the average strain for a particular lithology.
3. An accurate determination of the whole-rock strain of a conglomerate is more difficult. We suggest Fry analysis, using centres of the clasts of a particular size, even though it may not yield a classical Fry halo, nor necessarily be easy to find the best-fit strain ellipse. An alternative, if the fractions of all the component rock types in the conglomerate can be quantified and their average strains determined (e.g. via R_f-ϕ analysis), is to calculate the bulk strain as a weighted mean (the sum of the parts; Eq. (3)).
4. Using theory for inclusions in a matrix in pure shear, each having Newtonian properties, a simple equation can be written that relates the strain in a particular inclusion to the bulk strain, in terms of its viscosity ratio to the bulk viscosity (Eq. (1)). Applied to conglomerates, this allows viscosity contrasts to be computed from strain variations (Eq. (2)).
5. This inclusion–matrix model can be developed, via self-consistent mechanics, to show how the bulk viscosity of a multiphase mixture of spheres relates to its component parts, if their fractions and viscosity contrasts are known. For a two-phase mixture, the bulk viscosity is given by a quadratic equation. More complex polynomial relationships are found for multiphase mixtures, but simpler solutions arise for certain types of three- or four-phase mixtures. It may be possible to approximate a real conglomerate to one of these multiphase models, if the rock can be simplified into a finite number of component phases with Newtonian viscosity and definable volume fraction.
6. The first case study, the Port Askaig Tillite, is at one end of the spectrum of conglomerate types. It is a suspension of clasts with small volume fractions, in a dominant matrix fraction that is the least viscous material. Through strain measurements, we find that this rock, as a whole, behaves with very little difference from the tillite matrix, and so the strain measured by R_f-ϕ analysis of certain clasts is not a measure of the whole rock strain. From Fry analysis we determine a triple strain ratio of 4.8:2.6:1 for the whole rock, which is close to plane strain. Smaller strain values are determined, respectively, for quartzite, psammite and granite clasts, and their viscosity ratios (to matrix) range in value from 2 to 10.
7. The second case study, the Cesson Conglomerate, is at the other end of the conglomerate spectrum: a packed polymict conglomerate that we simplify into four component rock types: volcanics, granites, psammite, and semipelite. The bulk strain determined from Fry analysis is 7.3:3:1, also close to plane strain. The viscosity ratios of the different rocks, relative to the whole rock, occupy the range from 0.8 for semipelite (least) to 4.5 for granite (most). The whole rock behaves most similarly to volcanic or psammitic clasts, which are rheologically alike. Variations in three-dimensional strain emerge from the analyses of the different clast rock types, that may relate to viscosity contrasts, or reflect errors in strain analyses of real rocks whose clasts may not have been perfectly spherical or random, initially; or where the sample sizes have been smaller than ideal.
8. Results from the two case studies, together with comparable earlier studies, suggest that the viscosity contrasts among the common rock types fall within about one order of magnitude. These studies concern conglomerates of different type and deformation, and yet all produce surprisingly similar (small) values of viscosity ratios. This would be unlikely, if all the rock types had a general power-law rheology, because then their viscosities (and thus viscosity ratios) would vary according to strain rate

and P–T conditions. It leads us to conclude that the wide variety of common rock types found in conglomerates have mostly behaved as linearly viscous, during their progressive ductile deformation. This would appear to validate theoretical modelling of rocks and their structures as Newtonian, rather than power law, fluids.

9. Deformed conglomerates are useful not just for measuring strain. They also provide an ideal natural laboratory for deriving information on the rheology of many different rock types that have deformed in the same structural and crustal environment.

Acknowledgements

We are grateful to Alex Maltman, Mary Scott, Ian Fairchild and Mike Hambrey, for sharing information about field localities, and to Giles Droop for his help with petrographic identification. Thanks also go to Richard Lisle and Kurt Stüwe for their review and editorial comments, which helped us clarify and shorten the paper. This research was funded by NERC research grant GR3/10783 (J.E.T.), and a NERC Senior Research Fellowship (S.H.T.), which we gratefully acknowledge.

Appendix A. Inclusion–matrix theory

The expression derived by Gay (1968a) for the finite strain of a circular to elliptical inclusion in a matrix of contrasting viscosity, in plane pure shearing and with continuity at the inclusion/matrix interface, was given as:

$$\ln R_O = \ln R_S\{5/(3 + 2r)\}. \quad \text{(A1)}$$

R_O is the inclusion strain ratio (the X/Z stretch ratio), R_S is the bulk strain ratio (X/Z), and r is the viscosity ratio between the inclusion and matrix, which are both Newtonian viscous. This is a linear relationship of $\ln R_O$ and $\ln R_S$ (Fig. A1a), and so is insensitive to the effects of progressive inclusion ellipticity. It was considered incorrect (for two dimensions) by Bilby et al. (1975), who derived the following non-linear expression for the two-dimensional pure shear of a circular inclusion (strictly the cross-section of a circular cylinder):

$$\ln R_S = \ln R_O + \{(r - 1)(R_O - 1)/(R_O + 1)\}, \quad \text{(A2)}$$

as illustrated in Fig. A1b.

Eq. (A2) is now more widely accepted than Eq. (A1), for the finite strain of a circular inclusion, but it was noted by Gay (1976) that they have similar numerical solutions for geologically realistic values of bulk strain (R_S). Fig. A1 shows that the R_O vs. R_S values are virtually the same in Eqs. (A1) and (A2), for competent inclusions ($r > 1$) where $R_S \leq 10$. They are also a good approximation for incompetent inclusions, up to limits: for $r = 0.5$ up to $R_S \cong 6$ (a reasonable bulk strain for a conglomerate), and to higher

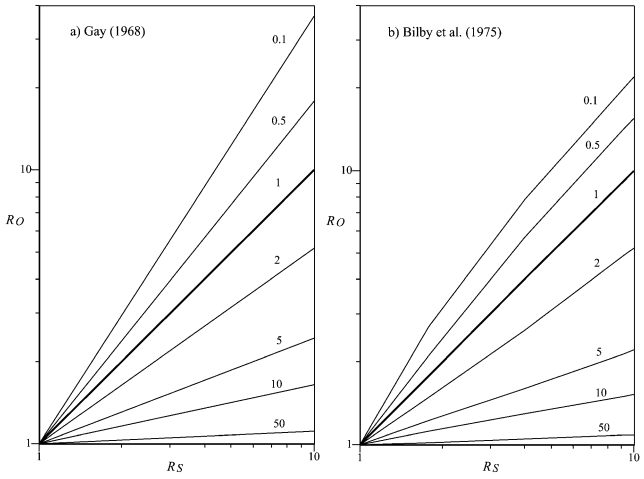

Fig. A1. Theoretical relationships between inclusion strain ratio (R_O) and bulk strain ratio (R_S). Numbers on the lines or curves are viscosity ratios of inclusion to matrix (r). (a) Eq. (A1), after Gay (1968a), is a linear $\ln R$ relationship. (b) Eq. (A2), after Bilby et al. (1975), appears similar to (a) and approximately linear, except for $r \ll 1$.

R_S for r values closer to one. Thus, we now favour using Eq. (A1) for practical geological applications in two dimensions, such as the conglomerates investigated in this paper.

The question of *three dimensions*, and which equation should be used for the sectional strain of spherical/ellipsoidal objects in pure shearing, needs to be addressed. We certainly do not envisage clasts in conglomerates to be circular cylinders, as two-dimensional analyses strictly dictate. However the inclusion–matrix studies cited above do not provide an explicit expression for the *finite strain* of a viscous ellipsoidal inclusion in a matrix, even for plane-strain pure-shear deformation. Eshelby (1957) (also Bilby et al., 1975) provided a relationship for the *infinitesimal* natural strain of a spherical object in pure shearing:

$$\epsilon_O/\epsilon_S = 5/\{3 + 2r\}, \quad \text{(A3)}$$

where ϵ_O is the inclusion strain, ϵ_S is the bulk or far-field strain, and r is the viscosity ratio defined above. This relationship is identical in form to Eq. (A1), and notably differs from the infinitesimal relationship in two dimensions derived from Eq. (A2) (Bilby et al., 1975), which is:

$$\epsilon_O/\epsilon_S = 2/\{1 + r\}. \quad \text{(A4)}$$

The fact that Eq. (A3) has the same form as Eq. (A1) might justify its use as the best *approximation* for finite strain of initially spherical inclusions in plane-strain pure-shear. However, the moment a spherical inclusion is deformed, the system cannot be treated as completely two-dimensional, even for bulk plane strain. Freeman (1987) showed that spherical inclusions with $r > 1$ (more competent) will become slightly prolate ellipsoids; those with $r < 1$ (incompetent) slightly oblate. The implications for strain analysis and for conglomerates were discussed by Freeman and Lisle (1987). We earlier attempted to assess

the inaccuracy arising from two-dimensional modelling that ignored these differences of strain in the third dimension (Treagus and Treagus, 2001), and concluded strain errors (in the *X*/*Z* ratio) of up to 5%. This suggests that the simple relationship given by Eq. (A1) is an acceptable approximation for moderate pure shear deformation of spheres in a matrix, for the purposes of modelling in this paper.

An additional advantage of Eq. (A1), when applied (as an approximation) to spherical objects in plane-strain pure-shear, is that the linear relationship of ln*R* operates for *any* of the three principal sections: not just for the *XZ* principal plane. R_O and R_S values in Eq. (A1) refer to *X*/*Z* strain ratios, assuming plane strain (and taking $Y = 1$ for both inclusion and matrix), but the same multiplying factor of $\{5/(3 + 2r)\}$ affects logarithms of all the principal strain ratios (e.g. *X*/*Y* and *Y*/*Z*) in the same way.

Appendix B. Models of multiphase viscous mixtures with spherical clasts

B.1. Two-phase mixtures

The bulk viscosity of a two-phase mixture that comprises two spherical phases, or one spherical phase in a continuous matrix phase, is modelled as follows (after Budiansky, 1965; Hill, 1965; Hashin, 1983; Treagus, 2002). The bulk infinitesimal strain (ϵ^*) is described as the weighted average of strains in phases 1 and 2 (ϵ_1, ϵ_2), with area or volume fractions (α_1, α_2), where $\alpha_1 + \alpha_2 = 1$:

$$\epsilon^* = \alpha_1\epsilon_1 + \alpha_2\epsilon_2. \tag{B1}$$

As given in full in Treagus (2002, eqs. 3–7), a similar average relationship can be written for stresses; and then by introducing viscosity terms, expressing strain rates over a small time increment as infinitesimal natural strains, and making substitutions, the following relationship is obtained for the bulk viscosity (μ^*) in terms of the two phase viscosities (μ_1, μ_2):

$$\mu^* = \mu_1 + \alpha_2(\mu_2 - \mu_1)(\epsilon_2/\epsilon^*), \tag{B2}$$

(cf. Hashin, 1983, eq. 3.1.3). For spherical clasts, ϵ_2/ϵ^* is defined in Appendix A, Eq. (A3) (after Eshelby, 1957) as:

$$\epsilon_2/\epsilon^* = 5/\{3 + 2\mu_2/\mu^*\}. \tag{B3}$$

Use of Eq. (B3) in Eq. (B2) then leads to a direct algebraic expression for the bulk viscosity of a two-phase mixture of spheres in pure shearing, in terms of the phase 2 fraction:

$$3\mu^{*2} + \mu^*\{(2\mu_2 - 3\mu_1) - 5\alpha_2(\mu_2 - \mu_1)\} - 2\mu_1\mu_2 = 0. \tag{B4}$$

This is the viscous equivalent to the result for a two-phase elastic composite, given by Hill (1965).

It is convenient to normalise the bulk viscosity with respect to phase 1, the least viscous or incompetent phase,

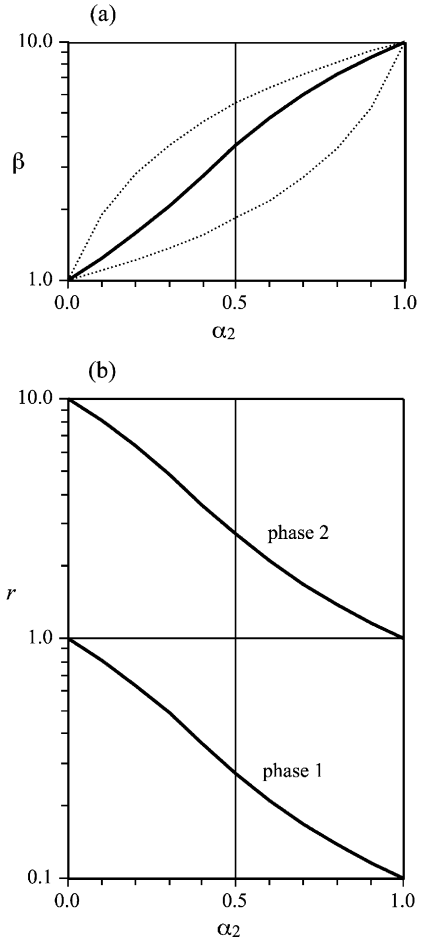

Fig. B1. The rheology of two-phase mixtures with spherical clast shape, in terms of α_2, the fraction of phase 2 (in 0.1 steps). See Appendix B.1. The phase viscosity contrast is $m = \mu_2/\mu_1 = 10$. (a) Normalised bulk viscosity of the mixture, β ($= \mu^*/\mu_1$), with the solid curves showing solutions to Eq. (B5) for each mixture. The upper and lower broken curves are the theoretical upper and lower bounds on β, given by Eq. (B7). (b) Viscosity ratios of each phase relative to the bulk viscosity, termed *r*.

which we define as $\beta = \mu^*/\mu_1$ (Treagus, 2002). Eq. (B4) can then be expressed as a quadratic equation in β, and if we write the two-phase viscosity ratio as $m = \mu_2/\mu_1$, we have:

$$3\beta^2 + \beta\{(2m - 3) - 5\alpha_2(m - 1)\} - 2m = 0, \tag{B5}$$

with the positive root defining β.

Solutions for β are illustrated for $m = 10$ and 100 in Treagus (2002, fig. 9), and are shown in Fig. B1a for $m = 10$. The broken upper and lower curves are the theoretical upper (U) and lower (L) viscosity bounds, defining the conditions of homogeneous strain and homogeneous stress, respectively (Treagus, 2002):

$$\mu^*_U = \alpha_1\mu_1 + \alpha_2\mu_2, \tag{B6a}$$

$$\mu^*_L = 1/\{\alpha_1/\mu_1 + \alpha_2/\mu_2\}. \tag{B6b}$$

Normalised relative to μ_1, these are:

$$\beta_U = \alpha_1 + \alpha_2 m \tag{B7a}$$

$$\beta_L = 1/\{\alpha_1 + \alpha_2/m\}. \tag{B7b}$$

It is seen in Fig. B1 that the normalised bulk viscosity (β) changes smoothly from one (where $\alpha_2 = 0$), to m (where $\alpha_2 = 1$), and is contained between the theoretical upper and lower bounds.

If we wish to define the phase viscosity ratio relative to the bulk viscosity (earlier termed r), for phase 1, $r = \mu_1/\mu^* = 1/\beta$; for phase 2, $r = \mu_2/\mu^* = m/\beta$. The r values for the $m = 10$ mixture are shown in Fig. B1b, to illustrate the way they change as the fractions of each phase change. Where there is a very small fraction of phase 2, its r value approaches m, because the bulk viscosity is approximately the same as μ_1. For fractions of $\alpha_2 = 0.2$ to 0.3, the bulk viscosity is weighted towards that of phase 1, and so phase 2 still shows a significant viscosity contrast. However, where $\alpha_2 = 0.4$ to 0.5, the bulk viscosity is roughly the geometric mean of the viscosities of the two phases, and so their r values become approximately $\mu_1/\mu^* \cong 1/\sqrt{m}$ and $\mu_2/\mu^* \cong \sqrt{m}$.

B.2. Multiphase mixtures, generalised

All the above principles for two-phase mixtures can be applied to an N-phase system. Thus, Eq. (B1) for averaging the bulk strain (ϵ^*) expands to:

$$\epsilon^* = \alpha_1\epsilon_1 + \alpha_2\epsilon_2 + \alpha_3\epsilon_3 + \ldots + \alpha_N\epsilon_N \tag{B8}$$

where α terms are area or volume fractions (equivalent, if statistically uniform) that sum to 1; and the ϵ terms are measures of natural strain in each numbered phase. The above expression for the average or bulk strain generalises to:

$$\epsilon^* = \sum_{n=1}^{N} \alpha_n\epsilon_n, \text{ where } \sum_{n=1}^{N} \alpha_n = 1. \tag{B9}$$

In what follows, we will order the phase numbers in increasing viscosity (competence) from 1 to N, with phase 1 (viscosity μ_1), the most incompetent phase, and phase N, the most competent.

As for two-phase systems, each phase can be considered as an inclusion phase with a strain that is a precise function of the bulk strain, related to the viscosity ratio and the inclusion shape. Taking the shape as spherical, we write the strain relationship for any nth phase, according to Eq. (B3):

$$\epsilon_n/\epsilon^* = 5/\{3 + 2\mu_n/\mu^*\}. \tag{B10}$$

Substituting this in Eq. (B9) leads to a general expression among the viscosity ratios for all N phases relative to the bulk viscosity, and the phase fractions:

$$\frac{1}{5} = \sum_{n=1}^{N} \frac{\alpha_n}{(3 + 2(\mu_n/\mu^*))}. \tag{B11}$$

To determine the expression for β involves the following substitutions:

$$\frac{\mu_n}{\mu^*} \equiv \frac{(\mu_n/\mu_1)}{\beta}. \tag{B12}$$

This leads to the expression:

$$\frac{1}{5} = \beta \sum_{n=1}^{N} \frac{\alpha_n}{(3\beta + 2(\mu_n/\mu_1))} \tag{B13}$$

Expansion of Eq. (B13) for N phases, and multiplication of all the terms, leads to a polynomial equation in β to the degree N, in terms of all the phase fractions and viscosity ratios to μ_1. For the two-phase system, this produces Eq. (B5), a quadratic equation in β. A cubic equation arises for a three-phase system, a quartic equation for a four-phase system, and so on to higher polynomials, and all these need to be solved by numerical means. It is not practical to write a general cubic or quartic expression in β for all possible three or four phase mixtures, but a few examples are given in the next sections.

Following the definitions for two phase mixtures given in Eqs. (B6) and (B7), the theoretical upper and lower bounds of the bulk viscosity of multiphase mixtures can be written:

$$\mu_U^* = \sum_{n=1}^{N} \alpha_n\mu_n, \tag{B14a}$$

$$\mu_L^* = \frac{1}{\sum_{n=1}^{N} \frac{\alpha_n}{\mu_n}} \tag{B14b}$$

or in normalised form:

$$\beta_U = \sum_{n=1}^{N} \alpha_n(\mu_n/\mu_1) \tag{B15a}$$

$$\beta_L = \frac{1}{\sum_{n=1}^{N} \frac{\alpha_n}{(\mu_n/\mu_1)}}. \tag{B15b}$$

As the bulk viscosity of any mixture must fall between these limiting values, these provide a useful check of the solutions for multiphase mixtures that yield complex polynomials in β.

B.3. Three phases in equal fraction

For a three-phase mixture that has equal fractions, we have $\alpha_1 = \alpha_2 = \alpha_3 = 0.33$. Taking phase 1 as the least viscous, we specify the viscosity contrasts of the other phases relative to this (μ_n/μ_1), with increasing values signifying increasing viscosity or competence. Eq. (B13)

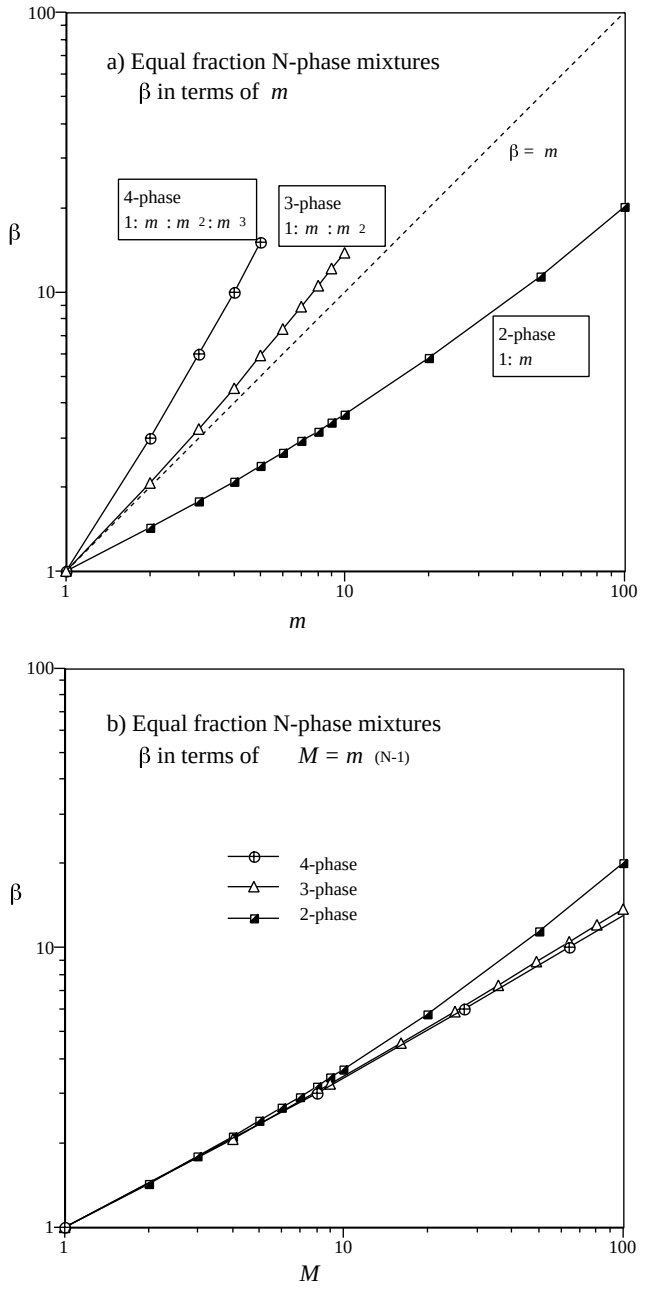

Fig. B2. Combined results for the normalised bulk viscosity (β) for two-, three- and four-phase mixtures that have equal phase fractions, and equal factorial changes in viscosity (m): see Appendix B.3. (a) β in terms of the m factor for the three models; (b) β in terms of the maximum viscosity contrast, M, where $M = m^{(N-1)}$.

then takes the form:

$$\frac{1}{5} = \frac{\beta}{3}\sum_{n=1}^{3}\frac{1}{(3\beta+2(\mu_n/\mu_1))}. \tag{B16}$$

We will further simplify, by considering a special kind of three-phase mixture which has an equal factor of increasing phase viscosity contrast, that can be expressed in the triple viscosity ratio (μ_1:μ_2:μ_3) of 1:m:m^2. This is a logical expansion of the earlier modelling of two-phase systems in terms of the two-phase viscosity contrast m. Expansion of Eq. (B16) then becomes:

$$\frac{3}{5} = \beta\left(\frac{1}{3\beta+2} + \frac{1}{3\beta+2m} + \frac{1}{3\beta+2m^2}\right). \tag{B17}$$

Multiplication and summation of terms eventually leads to the following cubic in β:

$$27\beta^3 + 3(1+m+m^2)\beta^2 - 8m(1+m+m^2)\beta - 12m^3 = 0 \tag{B18}$$

Numerical solutions for normalised bulk viscosity ($\beta = \mu^*/\mu_1$) are graphed in Fig. B2, for three-phase mixtures with m values of 2 to 10 (i.e. triple ratios of 1:2:4 to 1:10:100). Comparisons are also made with a two-phase 1:m mixture with equal phase fractions, and with an equal-fraction and equal factor four-phase mixture whose algebra is developed in the same way. The graph of β vs. m (Fig. B2a) shows that β is always slightly more than m, and so the bulk viscosity is slightly more than that of phase 2 (here the geometric mean of the three phases).

Alternatively, β can be considered vs. the *maximum viscosity ratio*, termed M (Fig. B2b), the ratio of the most to least viscous phase. For this three-phase system $M = m^2$. Comparisons are made in Fig. B2b with the comparable two-phase system ($M = m$) and four phase system ($M = m^3$). The logβ vs. log$M$ curves for the equal-factor three- and four-phase mixtures are almost the same, and approximately linear. These can be written as:

$$\beta \cong M^x = m^{x(N-1)}, \tag{B19}$$

where $x = 0.54$ for M of 1 to ~15, increasing to $x = 0.56$ for $M = 100$. We thus suggest $\beta \cong M^{0.55}$ as a good *general approximation* for any N-phase spherical mixture with equal phase fractions ($\alpha_n = 1/N$), and with equal factors of increasing viscosity (relative to the least viscous phase) in the range from 1 to M (where $M = m^{(N-1)}$).

B.4. Three-phase mixtures, where $\alpha_1 \neq \alpha_2 = \alpha_3$

Another type of simplified multiphase mixture is one comprising three phases, but with a variable α_1 fraction (the least viscous phase), and two different more viscous phases in equal fraction ($\alpha_2 = \alpha_3$). Thus $\alpha_1 = (1-2\alpha_2)$. The triple viscosity ratio of 1:10:100 will be considered, comparable with the three-phase 1:m:m^2 mixture in Appendix B.3. The general expression (Eq. (B13)) here expands to:

$$\frac{1}{5} = \beta\left[\alpha_1\frac{1}{3\beta+2} + \alpha_2\left(\frac{1}{3\beta+20} + \frac{1}{3\beta+200}\right)\right]. \tag{B20}$$

Multiplication and summation leads to the following

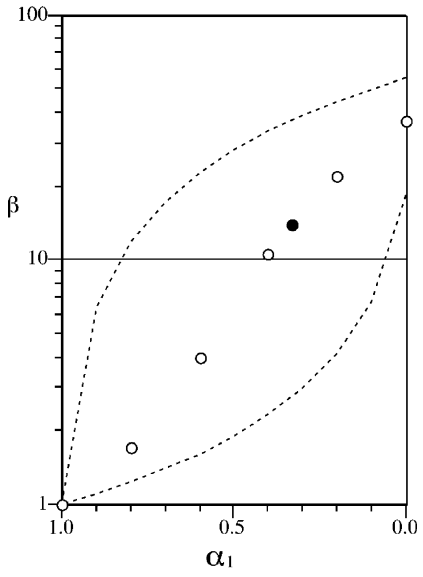

Fig. B3. A three-phase mixture, with two different phases in equal fraction ($\alpha_2 = \alpha_3$) in a least viscous phase with fraction α_1, and having a triple viscosity ratio of 1:10:100. Open circles are solutions to Eq. (B18) (Appendix B.4), plotted for examples at 0.2 intervals of α_1 (i.e. $\alpha_2 = \alpha_3 = 0.1$, 0.2, 0.3, 0.4 and 0.5). The solid circle is the equal-fraction three-phase mixture shown in Fig. B2 ($m = 10$; $M = 100$). The broken curves are the upper and lower bounds (cf. Fig. B1), but now according to Eq. (B22).

expression for β in terms of α_1:

$$\beta^3 + (90\alpha_1 - 17.67)\beta^2 + (1050\alpha_1 - 678.89)\beta - 444.44 = 0. \quad \text{(B21)}$$

The upper and lower bound values (Eq. (B15)) are:

$$\beta_U = 55 - 54\alpha_1 \quad \text{(B22a)}$$

$$\beta_L = \frac{1}{(0.055 - 0.945\alpha_1)} \quad \text{(B22b)}$$

Fig. B3 illustrates some numerical solutions for β for this example, plotted against the α_1 fraction. The symbol at the right hand ordinate ($\alpha_1 = 0$), shows the point where this mixture has no phase 1 fraction, and so becomes a two-phase mixture of phases 2 and 3 in equal fraction, with $m = 10$. (The β, β_U and β_L values are $10\times$ those given in Fig. B1 for $\alpha_2 = 0.5$.) The β curve roughly follows a midway curve of symmetry between the upper and lower bounds. Recalling the triple viscosity ratio (relative to phase 1) is 1:10:100, it can be seen that β (also relative to phase 1) is close to 10, i.e. the intermediate phase, when α_1 is approximately 0.4 (so $\alpha_2 = \alpha_3 = 0.3$). Where $\alpha_1 > 0.4$, the bulk viscosity is always smaller than phase 2, and so phases 2 and 3 are both relatively competent.

References

Bailey, E.B., 1917. The Islay Anticline. Quarterly Journal of the Geological Society of London 72, 132–164.

Bilby, B.A., Kolbuszewski, M.L., 1977. The finite deformation of an inhomogeneity in two-dimensional slow viscous incompressible flow. Proceedings of the Royal Society A355, 335–353.

Bilby, B.A., Eshelby, J.D., Kundu, A.K., 1975. The change of shape of a viscous ellipsoidal region embedded in a slowly deforming matrix having a different viscosity. Tectonophysics 28, 265–274.

Bjornerud, M.G., Boyer, B., 1996. Image analysis in structural geology using NIH Image. In: De Paor, D.G. (Ed.). Structural Geology and Personal Computers. Elsevier Science, Oxford, pp. 105–121.

Bons, P.D., Jessell, M.W., 1996. Image analysis of microstructures in natural and experimental samples. In: De Paor, D.G. (Ed.). Structural Geology and Personal Computers. Elsevier Science, Oxford, pp. 135–166.

Borradaile, G.J., Johnson, H.D., 1973. Finite strain estimates from the Dalradian Dolomitic Formation, Islay, Argyll Scotland. Tectonophysics 18, 249–259.

Budiansky, B., 1965. On the elastic moduli of some heterogeneous materials. Journal of the Mechanics and Physics of Solids 13, 223–227.

Burns, K.L., Spry, A.H., 1969. Analysis of the shape of deformed pebbles. Tectonophysics 7, 177–196.

Carter, N.L., Tsenn, M.C., 1987. Flow properties of continental lithosphere. Tectonophysics 136, 27–63.

De Paor, D.G. (Ed.), 1996. Structural Geology and Personal Computers. Elsevier Science, Oxford.

Dunnet, D., 1969. A technique of finite strain analysis using elliptical particles. Tectonophysics 7, 117–136.

Erslev, E., 1988. Normalized centre-to-centre strain analysis of packed aggregates. Journal of Structural Geology 10, 201–209.

Erslev, E., Ge, H., 1990. Least-squares centre-to-centre and mean object ellipse fabric analysis. Journal of Structural Geology 12, 1047–1059.

Eshelby, J.D., 1957. The determination of the elastic field of an ellipsoidal inclusion, and related problems. Proceedings of the Royal Society A 241, 376–396.

Flinn, D., 1956. On the deformation of the Funzie Conglomerate, Fetlar, Shetland. Journal of Geology 64, 480–505.

Freeman, B., 1987. The behaviour of deformable ellipsoidal particles in three-dimensional slow flows: implications for geological strain analysis. Tectonophysics 132, 297–309.

Freeman, B., Lisle, R.J., 1987. The relationship between tectonic strain and three-dimensional shape fabrics of pebbles in deformed conglomerates. Journal of the Geological Society 144, 635–639.

Fry, N., 1979. Random point distributions and strain measurement in rocks. Tectonophysics 60, 89–105.

Gay, N.C., 1968a. Pure shear and simple shear deformation of inhomogeneous viscous fluids. 1. Theory. Tectonophysics 5, 211–234.

Gay, N.C., 1968b. Pure shear and simple shear deformation of inhomogeneous viscous fluids. 2. The determination of the total finite strain in a rock from objects such as deformed pebbles. Tectonophysics 5, 295–302.

Gay, N.C., 1969. The analysis of strain in the Barberton Mountain Land, Eastern Transvaal, using deformed pebbles. Journal of Geology 77, 377–396.

Gay, N.C., 1976. The change of shape of a viscous ellipsoidal region embedded in a slowly deforming matrix having a different viscosity—a discussion. Tectonophysics 35, 403–407.

Hashin, Z., 1983. Analysis of composite materials—a survey. Journal of Applied Mechanics 50, 481–505.

Hill, R., 1965. A self-consistent mechanics of composite materials. Journal of the Mechanics and Physics of Solids 13, 213–222.

Hossack, J.R., 1968. Pebble deformation and thrusting in the Bygdin area (southern Norway). Tectonophysics 5, 315–339.

Huber-Aleffi, A., 1982. Strain determinations in the conglomeratic gneiss of the Lebendun nappe, Ticino, Switzerland. Ph.D. thesis, University of Zurich, Switzerland.

Kirkby, S.H., Kronenberg, A.K., 1987. Rheology of the lithosphere: selected topics. Reviews of Geophysics 25, 1219–1244.

Kohlstedt, D.L., Evans, B., Mackwell, S.J., 1995. Strength of the lithosphere:

constraints imposed by laboratory experiments. Journal of Geophysical Research 100, 17,587–17,602.

Leeder, M.R., 1982. Sedimentology: Process and Product. Chapman & Hall, London.

Lisle, R.J., 1979. Strain analysis using deformed pebbles: the influence of initial pebble shape. Tectonophysics 60, 263–277.

Lisle, R.J., 1985. Geological Strain Analysis. A Manual for the R_f/ϕ Technique. Pergamon Press, Oxford.

Lisle, R.J., Rondeel, H.E., Doorn, D., Brugge, J., van de Gaag, P., 1983. Estimation of viscosity contrast and finite strain from deformed elliptical inclusions. Journal of Structural Geology 5, 603–609.

McNaught, M., 1994. Modifying the normalized Fry method for aggregates of non-elliptical grains. Journal of Structural Geology 16, 493–503.

Ramsay, J.G., 1967. Folding and Fracturing of Rocks. McGraw-Hill, New York.

Ramsay, J.G., Wood, D.S., 1973. The geometric effects of volume change during deformation processes. Tectonophysics 16, 263–277.

Ramsay, J.G., Huber, M., 1983. The Techniques of Modern Structural Geology. Volume I. Strain Analysis. Academic Press, London.

Roach, R.A., Topley, C., Brown, M., Shufflebotham, M.M., 1986. Brioverian volcanism and Cadomian plutonism in the northern part of the Armorican massif. Pre-Conference Excursion Guide to I.G.C.P. 217 Meeting, Keyworth, Notts, UK, April 1–5 1986.

Rutter, E.H., 1993. The mechanics of natural rock deformation. In: Hudston, J.A. (Ed.). Comprehensive Rock Engineering. Pergamon Press, Oxford, pp. 63–92.

Shimamoto, T., Hara, I., 1976. Geometry and strain distribution of single-layer folds. Tectonophysics 30, 1–34.

Spencer, A.M., 1971. Late Precambrian Port Askaig Tillite in Scotland. Memoir of the Geological Society of London, No. 6.

Spencer, A.M., 1981. The late Precambrian Port Askaig Tillite in Scotland. In: Hambrey, M.J., Harland, W.B. (Eds.). Earth's Pre-Pleistocene Glacial Record. Cambridge University Press, pp. 632–636.

Treagus, S.H., 1999. Are viscosity ratios measurable from cleavage refraction? Journal of Structural Geology 21, 895–901.

Treagus, S.H., 2002. Modelling the bulk viscosity of two-phase mixtures in terms of clast shape. Journal of Structural Geology 24, 57–76.

Treagus, S.H., Lan, L., 2000. Pure shear deformation of square objects, and applications to geological strain analysis. Journal of Structural Geology 22, 105–122.

Treagus, S.H., Treagus, J.E., 2001. Effects of object ellipticity on strain, and implications for clast–matrix rocks. Journal of Structural Geology 23, 601–608.